The role of membrane destabilisation and protein dynamics in BAM catalysed OMP folding.

Paul White
University of Leeds
Samuel Haysom
University of Leeds https://orcid.org/0000-0002-8769-090X
Matthew Iadanza
University of Leeds
Anna Higgins
University of Leeds
Jonathan Machin
University of Leeds
Jim Horne
University of Leeds https://orcid.org/0000-0001-5260-2634
Bob Schiffrin
University of Leeds
Charlotte Carpenter-Platt
University of Leeds
James Whitehouse
University of Leeds
Kelly Storek
Genentech Inc
Steven Rutherford
Genentech Inc https://orcid.org/0000-0002-4758-4248
David Brockwell
University of Leeds https://orcid.org/0000-0002-0802-5937
Neil Ranson
University of Leeds https://orcid.org/0000-0002-3640-5275
Sheena Radford (s.e.radford@leeds.ac.uk)
University of Leeds https://orcid.org/0000-0002-3079-8039

Article

Keywords: outer membrane proteins (OMPs), β-barrel assembly machinery (BAM), OMP folding.

Posted Date: February 2nd, 2021

DOI: https://doi.org/10.21203/rs.3.rs-155135/v1

Version of Record: A version of this preprint was published at Nature Communications on July 7th, 2021.
See the published version at https://doi.org/10.1038/s41467-021-24432-x.

The role of membrane destabilisation and protein dynamics in BAM catalysed OMP folding

Paul White[1‡], Samuel F. Haysom[1‡], Matthew G. Iadanza[1•‡], Anna J. Higgins[1], Jonathan M. Machin[1], Jim E. Horne[1#], Bob Schiffrin[1], Charlotte Carpenter-Platt[1], James M. Whitehouse[1], Kelly M. Storek[2], Steven T. Rutherford[2], David J. Brockwell[1], Neil A. Ranson[1*], Sheena E. Radford[1*]

[1] Astbury Centre for Structural Molecular Biology, School of Molecular and Cellular Biology, Faculty of Biological Sciences, University of Leeds, Leeds, LS2 9JT, UK

[2] Department of Infectious Diseases, Genentech Inc., South San Francisco, CA 94080

[‡] Contributed equally

[•] Current affiliation: Scientific Computing Department, Science and Technology Facilities Council, Research Complex at Harwell, Didcot, OX11 0FA, UK

[#] Current affiliation: Department of Biochemistry, University of Oxford, Oxford, OX1 3QU, UK

*Correspondence: n.a.ranson@leeds.ac.uk; s.e.radford@leeds.ac.uk

Abstract

The folding of β-barrel outer membrane proteins (OMPs) in Gram-negative bacteria is catalysed by the β-barrel assembly machinery (BAM). How lateral opening in the β-barrel of the major subunit BamA assists in OMP folding, and the contribution of membrane disruption to BAM catalysis remain unresolved. Here, we use an anti-BamA monoclonal antibody fragment (Fab1) and two disulphide-crosslinked BAM variants (lid-locked (LL), and POTRA-5-locked (P5L)) to dissect these roles. Despite being lethal *in vivo*, we show that all complexes catalyse folding *in vitro*, albeit less efficiently than wild-type BAM. CryoEM revealed that while Fab1 and BAM-P5L trap an open-barrel state, BAM-LL contains a mixture of closed and contorted, partially-open structures. Finally, all three complexes globally destabilise the lipid bilayer, while BamA does not, revealing that the BAM lipoproteins are required for this function. Together the results provide new insights into the role of BAM structure and lipid dynamics in OMP folding.

Main

Outer membrane proteins (OMPs) in Gram negative bacteria are functionally diverse, but share a common β-barrel fold involving between 8 and 36 β-strands[1]. The folding and membrane insertion of OMPs is catalysed by the essential β-barrel assembly machinery (BAM)[2–4] which in *E. coli* comprises five proteins (BamABCDE). The major conserved subunit, BamA, is a 16-stranded Omp85 family member that contains five N-terminal polypeptide transport associated (POTRA) domains that extend into the periplasm to scaffold four lipoproteins BamB-E[5–8], all of which are required for maximally-efficient OMP folding[9,10]. BAM is essential for bacterial survival, highly conserved, and surface accessible via the extracellular loops of BamA, making the complex an attractive target for small molecule[11–13], peptide[14,15] and antibody-based antibiotics[16,17].

BAM exists in an ensemble of conformations, with one of the most notable differences between published structures occurring around the seam or 'lateral gate' involving β-strands 1 (β1) and 16 (β16) in the BamA barrel[6–8,18–20]. In the 'lateral-open' conformation, as captured by cryoEM of the intact complex[8] and X-ray crystallography of the BamACDE sub-complex[5,6], β1 and β16 are separated. In contrast, crystal structures of the intact BAM complex are in a 'lateral-closed' conformation in both in the absence[6,7] or presence of substrates[21,22], wherein β1 and β16 are hydrogen bonded, albeit with fewer hydrogen bonds than exist between the other strands in the barrel[1]. The POTRA domains are also dynamically organised, with motions of POTRA-5 being tightly correlated with gate conformation, with POTRA-5 plugging entrance to the BamA β-barrel lumen only in the lateral-open state[18]. These conformational changes are essential for cell viability as disulphide bonds that purportedly lock BamA in either conformation have a lethal phenotype that is rescued by reducing agent[6,19]. Such variants include those that lock the lateral gate closed (e.g. G433C/N805C linking β1 to β16[8,19], or E435C/S665C locking extracellular loop 1 (eL1) to eL6[6,19]), or those that lock the BamA lateral gate in an open conformation by introducing a disulphide bond between POTRA-5 and β-turn between β8 and β9 at the base of the barrel (e.g. G393C/G584C[6]). Disulphide bonds which restrict flexibility between POTRA domains 2 and 3 also impair growth[23]; how, or if, these motions correlate with structural changes at the BamA β-barrel is unclear.

Models of BAM-catalysed OMP insertion and folding broadly invoke two distinct roles for BAM (reviewed in[24]). Firstly conformational changes in BAM, and protein-protein interactions between BAM and substrate OMPs are thought to be involved in catalysing folding[25–29]. These models all involve a folding intermediate in which the C-terminal β-strand of the substrate is associated with BamA-β1, as supported by crosslinking[26,27], a recent cryoEM structure of a hybrid barrel formed between BAM and tBamA (the transmembrane domain of a BamA substrate)[29], and crystal structures of BAM covalently tethered to the C-terminal β-strands of OMP substrates OmpA and OmpLA[22]. Variations of these models include the

'barrel elongation'[25] and 'swing'[27] models which suggest that folding begins in the periplasm, and also 'budding' models[1,3,25] wherein OMPs are thought to enter the lumen of the BamA barrel and fold via sequential addition of β-hairpin units[26]. This is akin to the role proposed for the mitochondrial homologue Sam50 of the sorting and assembly machinery (SAM) complex[26]. An alternative model proposes that BAM may disorder its lipid environment, lowering the kinetic barrier to OMP folding, potentially allowing OMPs to fold and insert into the outer membrane without direct interaction with the β1-β16 seam. This 'BamA-assisted' model[18,30–32] is supported by molecular dynamics (MD) simulations which show lipid disordering and bilayer thinning by BamA[20,25,30–35], and by BAM-mediated distortion of a nanodisc[18]. Both protein dynamics and lipid disordering may act synergistically to maximise the efficiency of OMP folding, and different OMPs may depend on each effect to different degrees. However, little mechanistic insight is available, beyond that which has been inferred from the observation of a lethal phenotype.

Here, we investigate the roles of BAM structure/dynamics and membrane stability in OMP folding by exploiting two disulphide-locked variants termed lid-lock (LL) and POTRA-5-lock (P5L) which are lethal *in vivo*[6,19], and purportedly lock BamA's barrel closed and open, respectively. We also investigate a bactericidal Fab fragment (Fab1), that binds to eL4 of BamA[16]. We report cryoEM structures for the two disulphide locked BAM variants and the BAM-Fab1 complex, revealing that BAM-P5L and Fab1 stabilise a lateral-open conformation, whilst BAM-LL adopts both a lateral-closed state and a distorted, partially-open conformation. Despite being lethal *in vivo*, the two disulphide variants and the Fab1-BAM complex are all able to catalyse the folding of the 8-stranded OMPs OmpX and tOmpA (the transmembrane region of OmpA) *in vitro*, though less efficiently than wild-type BAM, and by combining Fab1 and disulphide-locking, BAM is further inactivated. We also demonstrate that all BAM variants studied lower the phase transition temperature of their lipid environment, but that BamA alone does not, providing direct experimental evidence that lipid disordering by BAM requires the presence of its lipoproteins. The results provide new insights into the structural features of BAM's catalytic mechanism and suggest that even subtle disruption of BAM activity may provide an effective route to the development of novel antibiotics.

Results

Disulphide-locked and Fab1-bound BAM can catalyse OMP folding in vitro

To assess the relationship between bacterial lethality and the catalytic ability of BAM we determined the *in vitro* folding activity of two paired cysteine mutations in BamA that are bactericidal[6,19]. In the BAM-P5L variant (BamA G393C/G584C)[6], tethering of POTRA-5 to the base of the BamA barrel is expected to stabilise a lateral-open conformation (**Fig. 1a**). By contrast, the BAM-LL variant, (BamA E435C/S665C)[19] is expected to lock eL1 to eL6, and stabilise a lateral-closed conformation (**Fig. 1b**). The BAM-LL and BAM-P5L variants were made in a BAM construct in which the two Cys of BamA that naturally form a disulphide bond (C690 and C700), are replaced with Ser (Cys-free BAM). This variant is able to complement WT BamA in *E. coli*[19,36] and has little effect on BAM-catalysed OMP folding rates *in vitro*[8]. We also investigated how a bactericidal anti-BamA binding antibody Fab fragment, known as Fab1[16,37], affects OMP folding *in vitro*. BAM-P5L, BAM-LL and the BAM-Fab1 complex were each reconstituted into liposomes comprised of *E. coli* polar lipids, and their ability to fold the 8-stranded OMPs, OmpX and tOmpA, in the presence of SurA was determined by SDS-PAGE band-shift assays[38]. In each case, BamA was folded (as judged by a band-shift relative to the boiled (denatured) BamA band) and all four BAM lipoproteins were present (**Supplementary Fig. 1)**. Interestingly, Fab1 formed a stable, SDS-resistant complex with BamA (**Supplementary Fig. 1b**), consistent with its IC_{50} of 0.095 nM determined for Δ*waaD E. coli*[16]. Disulphide bond formation in BAM-P5L and BAM-LL was confirmed by the lack of fluorescein-C5-maleimide labelling, and electrophoretic band-shifts in oxidising/reducing conditions (**Supplementary Fig. 2)**. Both tOmpA or OmpX do not fold spontaneously into the liposomes formed from *E. coli* polar lipids, but fold rapidly and efficiently into liposomes formed from the same lipids containing WT BAM (**Fig. 1c and d**). Remarkably, considering their *in vivo* lethality[6,16,19], the efficiency of folding and membrane insertion of tOmpA and OmpX is reduced, but not abolished, by BAM-P5L, BAM-LL and BAM-Fab1, with folding yields of ~50% for tOmpA and ~15-30% for OmpX after 3 hours at 25 °C (note that tOmpA folds more rapidly than OmpX with WT BAM) **(Fig. 1c and d, and Supplementary Fig. 3 and 4)**. Relative to WT BAM, the initial rates of folding for BAM-Fab1, BAM-LL and BAM-P5L ranged from 16-20% for tOmpA, and 8-29% for OmpX (**Fig. 1e and f, respectively, and Supplementary Table 1**). When the disulphide bond in BAM-P5L and BAM-LL is reduced with DTT, folding activity surpassed that of WT BAM. This effect was not observed for WT BAM, or Cys-free BAM (**Supplementary Fig. 5**). Folding into proteoliposomes containing BamA alone was much slower than observed with BAM-P5L, BAM-LL, or BAM-Fab1, with initial folding rates for both substrates reaching ~3% of that WT BAM, highlighting the importance of the accessory lipoproteins for efficient catalysis of folding of these OMPs[39]. Importantly, the inhibited BAM variants were able to fold their OMP substrates to 80-100% completion after 24 hours, whilst incubation with BamA alone resulted in folding yields of only 50% and 16% for tOmpA and OmpX, respectively, after 24

hours (note that both substrates were unable to fold into empty liposomes even on these extended timescales) (**Supplementary Table 2**). Collectively, these results show that although both Fab1 binding and disulphide-locking of BamA are lethal *in vivo*[6,16,19], the BAM-catalysed folding of OmpX and tOmpA is only partially inhibited *in vitro*.

Lid-locked BAM exists in two conformations

To understand the molecular basis of inhibition, we determined the structure of BAM-LL in DDM detergent micelles using cryoEM. We predicted, based on the lethality of this mutation and the crystal/cryoEM structures of BAM in its different conformational states[5–8], that the formation of a disulphide bond between C435 and C665 would trap BAM in a lateral-closed state (**Fig. 1b**). However, 3D classification of cryoEM data of this construct revealed two distinct, approximately equally populated, structures (**Fig. 2 and Supplementary Fig. 6**). The first structure (at 4.1 Å resolution) is similar to the crystal structure of intact BAM in the lateral-closed conformation, with pairing of β1 and β16 (**Fig. 2a,b**) and displacement of POTRA-5 from beneath the barrel (**Fig. 2c**). The second structure (at 4.8 Å) has β1 and β16 separated (**Fig. 2d, e**) and POTRA-5 occludes the periplasmic face of the BamA barrel (**Fig. 2f**), and is thus consistent with a lateral-open conformation. In all previous lateral-open structures[5,6,8], extracellular loop 1 (eL1) bends away from the BamA β-barrel, separating the lid-lock cysteine positions (C435 and C665) by ~20 Å. Given the unequivocal *in vitro* biochemical evidence for formation of the lid-lock disulphide (**Supplementary Fig. 2**), eL1 must be distorted to allow disulphide bond formation with eL6. However, poor resolution in this region of the map, itself indicative of mobility, prevented modelling of this new eL1 conformation. We therefore used molecular dynamics-based flexible fitting (MDFF)[40] to morph the lateral-closed BAM-LL atomic model into the density observed in the second conformation, whilst maintaining the disulphide link. This generated a chemically plausible loop conformation (**Fig. 2e**), but this is not constrained by the EM density. The difference between eL1 conformations in the two BAM-LL structures is striking, and suggests that this region must be highly malleable to allow disulphide bond formation within the BamA β-barrel. Interestingly, the 'contorted open' BAM-LL structure closely resembles a recent structure of WT BAM in saposin nanodiscs[22] in which eL1 adopts this inward conformation in the absence of disulphide tethering. In accord with this idea, eL1 can adopt a wide range of conformations in lateral-open BAM structures (**Supplementary Fig. 7**). Overall, these data suggest that the lid-lock disulphide biases the conformational ensemble toward a lateral-closed conformation, but cannot completely pull the conformational equilibrium over to that state, consistent with BAM adopting only the lateral-open state in DDM detergent[8].

Fab1-bound BAM and BAM-P5L adopt a lateral-open state

Inspired by the findings that MAB1 (and Fab1) binding is lethal *in vivo*[16] and also retards OMP folding rates *in vitro* (**Figure 1**), we next investigated the effect of Fab1 binding on the conformation of BAM using cryoEM. The structure of BAM in complex with a bactericidal molecule (Fab1) was solved in DDM micelles to 5.1 Å resolution. The cryoEM map contained unambiguous density for Fab1 bound to the extracellular region of BamA (**Fig. 3a, Supplementary Fig. 8**), and revealed that BAM is in a lateral-open conformation when bound to Fab1, as defined by the position of POTRA-5, the shape of the BamA β-barrel, and the orientation of β1 and β16 (**Fig. 3b and c**). The structure of Fab1 alone was also solved by X-ray diffraction to ~3.0 Å resolution and this structure was flexibly fitted into the EM density map **(Supplementary Table 3**). In agreement with mutagenesis data[16], Fab1 binds specifically to eL4 (**Fig. 3d) (**contributing 98% of the total interface area of 934 Å^2 as determined by PISA interface analysis[41]), and the complementarity determining regions (CDRs) bind to residues Y550, E554 and H555 in BamA (**Fig. 3e)**. Interestingly, a BamA-specific nanobody (nanoE6) has also been found to bind eL4 (involving E554) and also influences dynamics in the lateral gate[17]. However, since binding of Fab1 to BAM (and nanoE6 to BamA[17]) does not drastically alter the conformation of eL4 from that seen in lateral-closed structures, how Fab1 binding stabilises a lateral-open conformation remains obscure. Finally, we determined the cryoEM structure of BAM-P5L at lower resolution (10.3 Å; **Supplementary Figs. 9 and 10**), and although the conformation of the lateral gate is not clearly observed at this resolution (**Supplementary Fig. 10a**), POTRA-5 unambiguously occludes the BamA barrel suggesting that BAM-P5L is in a "lateral-open"-like state (**Supplementary Fig. 10b**). Cross-correlation of the BAM-P5L, WT BAM[8] (open) and BAM-LL (closed) density maps, as well as comparison of the shapes of the BamA barrel in the different structures add further evidence that BAM-P5L is indeed in a lateral-open state, as expected from the design of the Cys mutants, (**Supplementary Figure 10d,e**).

Fab1 binding to disulphide-locked BAM further inhibits OMP folding

As BAM can populate a lateral-open conformation in the presence or absence of Fab1, we determined the cryoEM structure of BAM-LL bound to Fab1 to ascertain whether Fab1 binding could further stabilise a lateral-open conformation, potentially further blocking the conformational changes required for BAM's catalytic action. In contrast with BAM-LL, the cryoEM structure of the BAM-LL:Fab1 complex (at 7.1 Å resolution) contains a single structure which is in a lateral-open conformation (**Fig. 4a, Supplementary Fig. 11**), consistent with Fab1 biasing BamA's conformational equilibrium towards a lateral-open state (**Fig. 4b**) in which POTRA-5 occludes the barrel (**Fig. 4c**). Further evidence for the lateral-

closed state being incompatible with Fab1 binding was observed by SDS-PAGE, where the SDS-resistant BamA-Fab1 band observed for WT BAM-Fab1 was weaker for BAM-LL-Fab1, with a compensating increase in the band corresponding to non-complexed BamA, suggestive of the BAM-LL-Fab1 complex being less stable under SDS-PAGE conditions (**Supplementary Fig. 12a**). Interestingly, since MAB1 binds to BAM in the *E. coli* OM[16], this suggests that a lateral-open conformation is formed *in situ* in the OM, consistent with previous data[36]. Conversely, the Fab1-bound BAM-P5L complex produces an SDS-resistant band, consistent with stable binding to its lateral-open state (**Supplementary Fig. 12b**). tOmpA and OmpX folding assays revealed that the addition of Fab1 to BAM-P5L or BAM-LL each resulted in increased inhibition, with folding yields of ~10-20% for tOmpA (**Fig. 4d, Supplementary Fig. 13a**) and 5-10% for OmpX (**Fig. 4e, Supplementary Fig. 13b**) after 3 hours at 25 °C, and initial folding rates of only 1-3% and 1-6% of that of WT BAM for tOmpA and OmpX, respectively (**Fig. 4f and g**). This additive inhibition could arise from a synergistic reduction in conformational dynamics within the BAM complex, or from Fab1 binding and disulphide locking inhibiting distinct mechanisms of BAM-mediated folding catalysis.

BAM lipoproteins mediate destabilisation of the lipid bilayer

In vitro studies have shown that spontaneous OMP folding rates and efficiencies are increased in membranes with decreased thickness, increased fluidity, or containing bilayer defects[42–45]. As well as directly interacting with its substrate OMPs[27,29], BAM is also thought to reduce the stability of the lipid bilayer to facilitate folding, due to asymmetry in the hydrophobic thickness of the BamA β-barrel (which is narrowest in the vicinity of the lateral gate)[18,32]. Evidence for membrane destabilisation has been provided by molecular dynamics (MD) simulations of BamA in lipid bilayers[20,24,25,30–35] and by cryoEM and MD simulations of BAM in nanodiscs formed from *E. coli* polar lipids[18]. To determine how the different conformational states of BAM affect bilayer stability more directly, we measured the effect of the different BAM complexes studied above on the lipid phase transition of liposomes formed from 1,2-dimyristoyl-*sn*-glycero-3-phosphocholine (DMPC, *di*$C_{14:0}$PC) using the fluorescent lipid probe laurdan (**Supplementary Fig. 14**), the fluorescence emission spectrum of which depends on lipid phase[46]. DMPC was chosen for these experiments as it undergoes a gel-liquid phase transition with a midpoint of ~ 24 °C, compared with ~ 3 °C for *E. coli* polar lipid[47] and BAM has been shown to be active in DMPC liposomes[48]. As expected, a phase transition for empty DMPC liposomes was observed at 24 °C (**Fig. 5a, see also Supplementary Fig. 15**). Interestingly, the transition phase temperature (T_m) was not affected by the presence of BamA alone (**Fig. 5a**), demonstrating that the asymmetric BamA β-barrel does not itself cause this global perturbation of the lipid bilayer, at least as judged by this assay. By contrast, in all proteoliposomes containing the full BAM complex,

regardless of whether that complex is inhibited, the gel-liquid phase transition occurred at a lower temperature (~22-23 °C) and over a broader temperature range (**Fig. 5b**). These results thus demonstrate that BAM disrupts bilayer stability independently of the structure of the β1-β16 seam and shows that the BamB-E lipoproteins are essential for this perturbation of the membrane.

Discussion

Protein-protein interactions between BAM and substrate OMPs, and lipid disordering have both been implicated as important features in BAM function[3,24], but how these different facets of BAM are balanced to enable OMP folding remained unclear. Here, we have used structural, biochemical and kinetic refolding analyses to dissect these two roles, at least for the 8-stranded OMPs, tOmpA and OmpX. BAM is well-known to be conformationally dynamic, with cryo-EM and X-ray structures capturing the complex in lateral-open[5,6,8] and lateral-closed[6,7,21,22] conformations, and a recent cryoEM, MD and single molecule FRET study demonstrating dynamics of the complex in nanodiscs[18]. Furthermore, recent X-ray structures have demonstrated that the C-terminal strand of the OMP substrates tOMPa and OMPLA forms an antiparallel β-strand pairing with lateral-closed BamA β1, possibly capturing an early stage intermediate in OMP assembly[22]. A recent cryoEM structure of a BAM:tBamA complex revealed that the tBamA substrate forms a β-strand pairing with lateral-open BamA β1 of BAM, whilst making a side-chain mediated interface involving BamA β16, to form a hybrid barrel[29] that presumably mimics a late-stage assembly intermediate. This observation is consistent with crosslinking studies of EspP[27] and LptD[28] to BAM, and Por1 to SAM[26]. Given these insights, it is perhaps unsurprising that trapping BamA in the BAM complex in an open or closed conformation by disulphide bonding has a profound effect on bacterial viability, akin to the observations found using nanobodies[17], small molecules and peptidomimetic antibiotics, which also have a lethal outcome[11,12]. Remarkably, we show here that this *in vivo* lethality masks a more subtle effect on BAM activity that is revealed by *in vitro* activity assays. Both disulphide-locking and Fab1 binding inhibit, but do not abolish, BAM-catalysed folding of tOmpA and OmpX *in vitro* **(Fig. 1, and Supplementary Tables 1 and 2)**. The finding that these inhibitory effects are distinct and additive (**Fig. 4)** highlights the importance of different, presumably parallel, facets of BAM action for OMP folding catalysis. Our cryoEM structures confirm that in solution, both BAM-P5L and Fab1 lock BamA in a lateral-open conformation (**Figs. 3, 4, and Supplementary Fig. 10)**. Presumably this prevents substrate access and pairing to BamA β1 which recent structures suggest initially occurs to a lateral-closed conformation[22]. It may also inhibit substrate binding by occlusion of entry to the BamA barrel by POTRA-5. Consistent with this, it has recently been shown that the BAM substrate, RcsF, binds in the lumen of the BamA β-barrel only in the lateral-closed conformation[21], and that the essential mediator of

LPS assembly, LptD, contacts the internal lumen of BamA during folding[28]. An inability to assemble larger and essential BAM-dependent substrates, such as LptD, could explain why disulphide locking/Fab1 binding are lethal *in vivo*[6,16,19], despite smaller OMPs potentially remaining able to fold and insert into the OM, albeit more slowly than with WT BAM. For the latter OMPs, lethality may result from a reduced flux through the OMP biogenesis pathway when BAM is impaired, inducing cell envelope stress caused by accumulation of unfolded OMPs in the periplasm. Indeed, increased envelope stress was observed upon addition of MAB1 to Δ*waaD E. coli*[16]. Moreover, a small molecule inhibitor of the regulator of sigma E protease (RseP)[49], that is a key component of this pathway, has a lethal outcome by blocking the σ^E stress response that normally responds to envelope stress by increasing BAM expression[50], decreasing OMP expression[51], and increasing protein degradation[52]. The extent to which the folding of larger OMPs is inhibited by the BAM variants examined here remains unclear, but we speculate that for these proteins there could be a greater dependence on a direct interaction with BAM for successful insertion and folding, with BAM being unable to destabilise membranes sufficiently to allow larger OMPs to fold solely via this route.

Despite the apparent incompatibility of BAM-LL's disulphide bond and a lateral-open conformation[6,8], both open-like and closed structures are present in approximately equal populations in solution. The BAM-LL structures presented here thus provide direct evidence that at least β1 and β2 of BamA are malleable in the lateral-open state, being able to bend inwards towards the barrel lumen (**Supplementary Fig. 7**). Such plasticity appears to be functionally relevant, especially considering the more severe outward motion observed when BAM is engaged with tBamA as a substrate[29] (**Supplementary Fig. 7**). Such an extended conformation would presumably be impossible in BAM-LL, perhaps explaining the partial inhibitory effects observed here for OmpX and tOmpA. Superposition of all the lateral-open BAM structures reported to date thus support a model in which the N-terminal half of the BamA barrel is conformationally dynamic, whilst the C-terminal half provides a stable scaffold that supports these functionally important conformational changes.

Lipid destabilisation by BAM has been proposed previously as a potentially important facet of the catalysis of OMP folding and insertion into the OM[3,25,53]. This has been supported by MD simulations that reveal destabilisation of the membrane surrounding BamA[20,24,25,30–35], and a recent cryoEM structure of BAM in a nanodiscs containing *E. coli* polar lipids that shows distortion of the bilayer adjacent to the lateral gate[18]. Whilst these effects are localised to the BamA barrel, the laurdan fluorescence data provide direct biochemical evidence that BAM causes global destabilisation of a bilayer, as revealed by a reduction in the lipid phase transition temperature of DMPC liposomes (**Fig. 5**). They also reveal that this is mediated by lipoproteins BamB-E, since BamA alone had no discernible effect. This is consistent with cryoEM structures which have identified interactions between BamB, BamD and BamE and detergent micelles[8] as well as with lipid in nanodiscs[18], whilst BamC is

thought to span the membrane necessary for surface exposure of the two C-terminal helix-grip domains[54]. In addition to the roles of BamB-E in substrate recognition[15,55], in mediating BAM oligomerisation into 'precincts'[56], and coordinating conformational changes in BamA[36,57], the results presented here highlight the importance of these lipoproteins in mediating changes in membrane stability.

In summary, the results presented allow different facets of BAM-mediated catalysis of OMP folding and membrane insertion to be discerned. By structural analysis of Fab1-bound and two different disulphide locked BAM complexes we reveal a remarkable structural malleability of the BamA barrel, and show that interconversion between these different structures is not essential for folding and membrane insertion of the 8-stranded tOmpA and OmpX substrates *in vitro*. In addition, we provide direct biochemical evidence that BAM causes global destabilisation of a lipid bilayer and reveal that this is not endowed by asymmetry in the depth of the BamA barrel, but instead requires the presence of BamB-E, demonstrating a new role for its lipoproteins. Finally, by demonstrating a significant, but reduced folding capacity of the Fab1-bound and disulphide-locked BAM variants *in vitro*, we provide evidence in support of models that suggest that bacterial viability depends on a delicate balance between the rates of OMP synthesis and their chaperone-dependent delivery to BAM, with the catalytic power of BAM to insert OMPs into the OM. Perturbing this balance thus offers exciting opportunities to create new antibacterial agents by targeting the different protein complexes required for OMP biogenesis.

Methods

Expression and purification of WT and disulphide-locked BAM complexes

BAM-LL (BamA(E435C/S665C/C690S/C700S)BCDE-His_6) and BAM-P5L (BamA(G393C/G584C/C690S/C700S)BCDE-His_6) in a pTrc99a vector were generated using Q5 site-directed mutagenesis (New England BioLabs) using plasmid pJH114 (kindly provided by Harris Bernstein[58]) as a template. WT BAM, BAM-LL and BAM-P5L were expressed in *E. coli* BL21(DE3) cells and were purified from the membrane fraction using a combination of Ni-affinity and size exclusion chromatography, as described previously[8].

Expression and purification of BamA, OmpX and tOmpA

BamA, OmpX and tOmpA were expressed as inclusion bodies in *E. coli* BL21(DE3) cells, using a procedure modified from McMorran *et al.*[50]. Briefly, inclusion bodies were solubilised in 25 mM Tris-HCl pH 8.0, 6 M guanidine-HCl and were centrifuged (20,000 *g*, 20 min, 4 °C) to remove remaining insoluble material. The solubilised inclusion bodies were purified by SEC using a Superdex 75 HiLoad 26/60 column (GE Healthcare) for tOmpA and OmpX, and Sephacryl 200 26/60 column for BamA, equilibrated in 25 mM Tris-HCl pH 8.0, 6 M guanidine-HCl. For folding experiments, OmpX and tOmpA were buffer exchanged into Tris-buffered saline (TBS, 20 mM Tris-HCl, 150 mM NaCl) pH 8.0, 8 M urea using Zeba™ Spin Desalting Columns, 7k MWCO, 0.5 mL (Thermo Scientific). BamA was refolded in LDAO detergent prior to reconstitution into proteoliposomes, as described previously[59].

Refolding of BamA

BamA was refolded as described by Hartmann *et al.*[59]. Briefly, BamA added dropwise into ice-cold 50 mM Tris-HCl pH 8.0, 300 mM NaCl, 500 mM arginine, 0.5% (*w/v*) LDAO, 10 mM DTT whilst rapidly stirring. Following 24 hours incubation, BamA was dialysed against 50 mM Tris-HCl pH 8.0, 0.1% (*w/v*) LDAO overnight before loading on a 5 mL HiTrap Q (GE Healthcare) anion exchange column and eluting in a NaCl gradient. Folded BamA was separated from unfolded and degraded BamA, as judged by SDS-PAGE, and used for reconstitution into liposomes containing *E. coli* polar lipid or DMPC, as required.

Expression and purification of SurA

SurA with an N-terminal 6x His-tag and a TEV cleavage site was expressed and purified using a modified protocol described previously[60]. Briefly, SurA was expressed in *E. coli* BL21(DE3) cells and was purified on a 5 mL HisTrap FF column (GE Healthcare). SurA was denatured on-column in 25 mM Tris-HCl pH 7.2, 6 M guanidine-HCl, washed in the same

buffer and then refolded on-column in 25 mM Tris-HCl pH 7.2, 150 mM NaCl, 20 mM imidazole before elution in 25 mM Tris-HCl pH 7.2, 150 mM NaCl, 500 mM imidazole. The His-tag was cleaved by addition of His-tagged TEV protease and 14.3 mM 2-mercaptoethanol, produced as previously described[31], and the cleaved His-tag and TEV protease were removed on a 5 mL HisTrap FF column. Purified SurA was dialysed against 5 L TBS pH 8.0, concentrated to ~200 µM using Vivaspin 20 MWCO 10 kDa concentrators (Sartorius, UK), aliquoted, snap-frozen in liquid nitrogen, and stored at -80 °C.

Monoclonal antibody Fab production

Fabs were cloned and expressed in *E. coli* as previously described[61,62]. Cell paste containing the expressed Fab was resuspended in PBS buffer containing 25 mM EDTA and 1 mM PMSF. The mixture was homogenised and then passed twice through a microfluidiser. The suspension was then centrifuged at 21,500 *g* for 60 min. The supernatant was loaded onto a Protein G column equilibrated with PBS at 5 mL/min. The column was washed with PBS to baseline and proteins were eluted with 0.6% (*v/v*) acetic acid. Fractions containing Fabs, assayed by SDS-PAGE, were pooled and loaded onto a 50 mL SP Sepharose column equilibrated in 20 mM MES, pH 5.5. The column was washed with 20 mM MES, pH 5.5 for 2 column volumes and the protein was then eluted with a linear gradient to 0.5M NaCl in the same buffer. For final purification, Fab-containing fractions from the ion exchange column were concentrated and run on a Superdex 75 size exclusion column (GE Healthcare) in PBS buffer.

Reconstitution of BAM complex variants and BamA into *E. coli* polar lipid proteoliposomes

E. coli polar lipid extract, purchased as powder from Avanti Polar Lipids (Alabaster, AL), was dissolved in 80:20 (*v/v*) chloroform/methanol at 20 mg/mL. Appropriate volumes were dried to thin films in clean Pyrex tubes at 42 °C under N_2 gas, and were further dried by vacuum desiccation for at least 3 hours. WT BAM, BAM-LL and BAM-P5L in TBS pH 8.0, 0.05% (*w/v*) DDM were mixed with *E. coli* polar lipid extract films solubilized in TBS pH 8.0, 0.05% (*w/v*) DDM in a 1:2 (*w/w*) ratio. For formation of BAM-Fab1 proteoliposomes, a 2-fold molar excess of Fab1 was added to WT BAM, BAM-P5L or BAM-LL in TBS pH 8.0, 0.05% (*w/v*) DDM before mixing with lipid. For BamA proteoliposomes, refolded BamA was added to *E. coli* polar lipid films solubilised in TBS pH 8.0, 0.1% (*w/v*) LDAO in a 1:2 (*w/w*) ratio. Empty liposomes were prepared by mixing lipid with an equivalent volume of buffer. To remove detergent and promote liposome formation, the mixtures were dialyzed against 2 L of 20 mM Tris-HCl pH 8.0, 150 mM KCl using 12-14 kDa MWCO D-Tube™ Maxi Dialyzers (Merck) at room temperature for 48 hours with a total of four buffer changes. Following dialysis, the

proteoliposomes were pelleted twice by ultracentrifugation at 100,000 *g* for 30 mins at 4 °C (the supernatants referred to as wash 1 and wash 2 in Supplementary Figures) and were resuspended in TBS pH 8.0. Protein concentration was determined using a BCA assay (ThermoScientific) and successful reconstitution was determined by SDS-PAGE.

Fluorescein-C5-maleimide labelling of free thiols in BAM disulphide variants

WT BAM, BAM-LL and BAM-P5L proteoliposome preparations (containing 5 µM BAM) in TBS pH 8.0 were treated with 1 mM TCEP or 0.1 mM diamide, along with an untreated control, for 45 mins at room temperature. The proteoliposomes were then diluted 10-fold into TBS pH 7.5, 8 M urea containing 100 µM fluorescein-C5-maleimide and were incubated overnight at 25 °C. The products of the labelling reaction were then analysed by SDS-PAGE on 15 % (*w/v*) acrylamide/bis-acrylamide (37.5:1) Tris-tricine SDS-PAGE gels run at 60 mA per gel for 90 mins at 25 °C, and imaged under 460 nm light using an Alliance Q9 Advanced gel doc (UVITEC, Cambridge, UK). Subsequently gels were stained with Coomassie Blue to visualise all protein bands.

BAM-mediated folding of OMPs by SDS-PAGE band-shift assays

Solutions of 20 µM tOmpA or OmpX denatured in TBS pH 8.0 containing 8 M urea were diluted 5-fold into a 20 µM solution of SurA. This mixture was then immediately diluted 2-fold into BAM, BamA or empty proteoliposomes to initiate the folding reaction, maintained at 25 °C. Final concentrations were 1 µM BAM, 2 µM tOmpA/OmpX, 10 µM SurA, 0.8 M urea in TBS pH 8.0. DTT was included in the relevant folding reactions at a final concentration of 25 mM. Samples of the folding reaction were taken periodically and were quenched in SDS-PAGE loading buffer (final concentrations: 50 mM Tris-HCl pH 6.8, 10% (*v/v*) glycerol, 1.5% (*w/v*) SDS, 0.001% (*w/v*) bromophenol blue). The samples, including a boiled control (10 mins at > 95 °C), were run on 15 % (*w/v*) SDS-PAGE gels as described above. The gels were stained in InstantBlue™ (Experion) and were imaged using an Alliance Q9 Advanced gel doc (UVITEC, Cambridge, UK). Folded and unfolded band intensities were quantified using ImageJ software (Fiji) and were plotted as a fraction folded ($I_F/(I_F+I_{UF})$) against time. Folding data were fitted to a single exponential function in Igor Pro (V8.04) and initial rates calculated by applying a linear fit to data within the first 5% of the time-course (540 seconds).

CryoEM grid preparation

Samples for grid preparation were prepared as follows. Purified BAM-LL or BAM-P5L in 50 mM Tris-HCl pH 8.0, 150 mM NaCl and 0.05% (*w/v*) DDM were diluted to 3.3 mg/mL or 2.3

mg/mL, respectively. For the BAM-Fab1 complex, purified WT BAM was mixed with a 2-fold molar excess of Fab1 and run on a Superdex 200 10/300 column in TBS pH 8.0, 0.05% (*w/v*) DDM to isolate a stoichiometric complex from excess free Fab1. Fractions corresponding to the complex were concentrated to 4.8 µM in Vivaspin 500 concentrator MWCO 30k (Sartorius). To assemble the Fab1-bound BAM-LL complex, stock solutions of purified BAM-LL and Fab1 were first diluted to 5.9 µM in 20 mM Tris-HCl pH 8.0, 150 mM NaCl and 0.05% (*w/v*) DDM and mixed in a 1:1 molar ratio, before dilution in detergent-free buffer to a total protein concentration of 0.9 mg/mL and a total DDM concentration of 0.03% (*w/v*). The detergent concentration was lowered to combat a tendency for very thin ice on the resulting grids.

CryoEM grids were prepared as follows. For the BAM-Fab1 complex, 4 µL protein was applied to gold UltrAUfoil R2/2 200 mesh grids, previously glow discharged for 60 sec at 20 mA in a GlowQube Plus (Electron Microscopy Sciences) in the presence of amylamine vapor. For BAM-LL, BAM-P5L and BAM-LL in complex with Fab1, 3 µL of sample was applied to copper QUANTIFOIL R1.2/1.3 300 mesh, copper QUANTIFOIL R0.6/1 400 mesh and gold UltrAUfoil R1.2/1.3 300 mesh grids (Electron Microscopy Sciences), respectively, that were previously glow discharged for 30 sec at 60 mA in a GlowQube Plus (Electron Microscopy Sciences). Grids were blotted for 6 sec with Whatman #1 filter paper at 4 °C and 80-100% relative humidity, before plunge freezing in liquid ethane using a Vitrobot Mark IV (ThermoFisher).

CryoEM Imaging

Data were collected on a 300 KeV Titan Krios (ThermoFisher) EM in the Astbury Biostructure Laboratory in automated fashion using EPU software (ThermoFisher). Micrographs were recorded on an energy-filtered K2 detector (Gatan inc.) in counting mode, using a 100 µm objective aperture. For BAM-LL, 6,456 micrographs were collected from a single grid over two sessions. For the Fab1-bound BAM-LL complex, 2,780 micrographs were collected from a single grid. For BAM-P5L, two grids were imaged in separate sessions, resulting in 2150 total micrographs. For the BAM-Fab1 complex, a single grid was imaged over three sessions, resulting in 4197 total micrographs. Full data collection parameters for each sample are shown in **Supplementary Table 4.**

Image Processing

All processing was performed in RELION 3.0[63] (BAM-LL, BAM-Fab1, Fab1-bound BAM-LL) or 3.1[64] (BAM-P5L) unless otherwise stated. Dose-fractionated micrographs were motion-corrected and dose-weighted by MotionCor2[65], before estimation of contrast transfer function parameters by Gctf[66] using the motion corrected and dose-weighted micrographs,

apart from the BAM-Fab1 complex where motion corrected, but non-dose weighted, micrographs were used.

For BAM-LL, the two datasets were initially processed separately in a similar manner (**Supplementary Fig. 6).** For dataset 1, 299,458 particles were first picked using the general model in crYOLO 1.3.5[67], and extracted in 300 pixel (321 Å) boxes with two-fold binning, before removal of false positives through two rounds of 2D classification. The resulting 234,598 particles were then used to generate an initial model by stochastic gradient descent[68], which was used as the starting model for a 3D classification. Two high resolution classes corresponding to different conformations of BAM-LL were obtained, one termed lateral-closed (86,615 particles) and one lateral-open (83,803 particles). Particles corresponding to each class were then re-extracted unbinned, and autorefined with a mask excluding bulk solvent. After masking and sharpening, resolutions of 5.0 Å (lateral-closed) and 5.9 Å (lateral-open) were obtained. Processing of dataset 2 proceeded similarly and resulted in comparable resolutions for both conformations. To achieve higher resolution, one round of CTF refinement followed by Bayesian polishing were then employed for each dataset, following which the particles corresponding to the same conformation were combined, resulting in 160,118 lateral-closed and 141,612 lateral-open particles. Finally these particle stacks were subject to separate non-uniform refinements in cryoSPARC v2.2.0[68,69]. Masking and sharpening of the resulting half-maps in RELION resulted in resolutions of 4.1 Å (lateral-closed) and 4.8 Å (lateral-open). B-factors of -107 $Å^2$ and -127 $Å^2$ were applied to the final lateral-closed and lateral-open reconstructions, respectively. Local resolution was estimated using RELION.

For the BAM-Fab1 complex (**Supplementary Fig. 8**), particles were autopicked in RELION 3[63] using class averages from a previous reconstruction[8] filtered to 30 Å as search templates. Individual particles were extracted in 350 pixel (374.5 Å) boxes and culled with multiple rounds of 2D and 3D classification. The resulting particle stack containing 131,853 particles was further refined using the non-uniform refinement function in CryoSPARC v2.2.0[68,69]. The reconstruction was performed on independent subsets and final resolution of 5.2 Å determined by 'gold standard' FSC[70]. A B-factor of -167 $Å^2$ was applied to the final reconstruction.

For BAM-P5L (**Supplementary Figs. 9 and 10**), particles were picked in crYOLO 1.4.1 using the general model. For dataset 1: 41, 316 particles were picked and extracted in a 280 pixel (300 Å) box, for dataset 2: 54, 532 particles were picked and extracted into 352 pixel (300 Å) boxes. Both used twofold binning. The extracted particles were combined into a single dataset and the resulting 95,848 particles passed through 2D classification. The best 21, 483 particles were used to construct an initial model by stochastic gradient descent[68], which was used as a reference for 3D classification of the 43,280 good particles from 2D

classification. The resulting 24, 101 particles were autorefined, and re-extracted as unbinned particles and subject to 3D classification using the autorefined model as the reference. The resulting 19,044 particles were autorefined with a mask to a resolution of 10.3 Å. A B-factor of -671 Å^2 was applied to the final reconstruction

For the Fab1-bound BAM-LL complex (**Supplementary Fig. 11**), particles were picked in crYOLO 1.4.1 using a model trained with 11 handpicked micrographs spanning the defoci range. The resulting 162,844 particles were extracted in 300 (321 Å) pixel boxes with twofold binning. One round of 2D classification was used to cull the particle set to 108,096 particles which was then subject to 3D classification, using an initial model generated by stochastic gradient descent[68] from the best 32,645 particles in that stack as a template. From this 3D classification run, only one conformer was observed, corresponding to a lateral-open, BAM-LL bound to Fab1. The 71,675 particles in the highest resolution class were autorefined, re-extracted as unbinned particles and subject to 3D classification using the autorefined model as the reference, further culling the particle stack. Autorefinement and sharpening of the resulting 61,777 good particles gave a resolution of 7.3 Å. Finally, one round of CTF refinement followed by Bayesian polishing was carried out, and the resulting particle stacks were subject to non-uniform refinement in cryoSPARC v2.2.0[68,69]. Masking and sharpening of the resulting half-maps in RELION resulted in a resolution of 7.1 Å. A B-factor of -274 Å^2 was applied to the final reconstruction.

CryoEM model building and refinement

For LL-BAM in the lateral-closed cryoEM map, an existing crystal structure of intact BAM in a lateral-closed conformation (PDB ID: 5D0O[6]) was first edited to both remove the two natural cysteines in BamA and to insert the lid-lock disulphide bond. This starting model was fitted to the density as a rigid body in Chimera[71], before performing several iterations of real-space refinement in PHENIX 1.14[72] with secondary structure restraints followed by manual refinement in COOT[73], until satisfactory geometry and fit between model and map was obtained as assessed using MolProbity[74]. The extracellular region of eL6 ($BamA_{675-702}$), C-terminal globular domains of BamC ($BamC_{89-344}$), and regions at the chain termini of BamABCDE were insufficiently resolved and were not modelled. The final model contains $BamA_{24-675,\ 702-810}$ $BamB_{31-391}$, $BamC_{30-85}$, $BamD_{27-244}$, $BamE_{29-111}$.

As the resolution of the other structures was insufficient for the above approach, Molecular Dynamics Flexible Fitting (MDFF)[40] was used to flexibly fit these conformations. For BAM-LL lateral-open, cascade MDFF (cMDFF) simulations of the lateral-closed atomic model with BamA truncated after residue 809 were first used to derive an initial fit to the lid-lock lateral-open cryoEM map. Here, a series of Gaussian blurred density maps were generated using the volutil function in VMD (halfwidths σ = 0, 1, …, 6 Å). The atomic model was then simulated in vacuum and subject to an external potential derived from most blurred density

map, causing it to be flexibly fit into the density. 2 ps of minimisation followed by 100 ps of equilibration were run with a gscale of 1.0 defining the strength of the external potential derived from the density map. Consecutive 100 ps simulations were then run into maps of decreasing blurring, where the end coordinates from the previous simulation were used as input for the next, until reaching the unblurred map. At each step, isomerism, chirality and secondary structure restraints were applied. Several repeats were run, taking advantage of the stochastic nature of the simulation to generate different fits. Additionally, a second MDFF simulation was also run into the unblurred map using PDB-5LJO[8] as a starting model, to derive better conformations for $BamA_{720-734}$ and $BamA_{807,\ 808}$. These models were then manually combined to give best mainchain fit to the density, before minimising against the unblurred map for 40 ps. In the combined model, $BamA_{429-440}$, corresponding to eL1 and the extracellular sides of β1 and β2, was fitting into micelle density rather than protein density due to the low resolution in this region. A final set of 500 ps MDFF simulations were therefore run with this combined model against the unblurred map, in which $BamA_{429-440}$ was not subject to the external potential. The best fitting structure from these runs was then minimised for 40 ps against the unblurred map and real space refined in PHENIX 1.14[72] with secondary structure restraints to generate the final atomic model.

For the Fab1-bound wild-type BAM complex, an initial model was created from the BAM complex PDB entry 5LJO[8], with $BamA_{687-700}$ from 5EKQ[5], and the Fab1 crystal structure determined here (PDB 7BM5). The C-terminal globular domains of BamC were truncated, leaving only the lasso[75] region (residues 25-83) resulting in a starting model containing $BamA_{24-806}$, $BamB_{22-392}$, $BamC_{25-83}$, $BamD_{26-243}$, and $BamE_{24-110}$. The starting model was fitted into each EM density as a rigid body using UCSF Chimera[71] and flexibly fit using cMDFF[40]. This was followed by real space refinement in PHENIX 1.14[72] using secondary structure restraints to generate the final atomic model, with the Fab1 crystal structure used as a reference model to generate additional restraints.

For the Fab1-bound lid-locked BAM complex, the final lid-locked lateral-open structure and the Fab1 crystal structure were rigid body fitted into the EM density using UCSF Chimera and flexibly fit using a round of MDFF into the unblurred map. This was followed by real space refinement in PHENIX 1.14 with secondary structure restraints to generate the final atomic model, with the Fab1 crystal structure and the final lid-locked lateral-open structures used as reference models to generate additional restraints. During the simulation eL1 of BamA ($BamA_{429-440}$) was not subject to the external potential to prevent overfitting to micelle density in this region. Model building statistics for all cryoEM conformers are shown in **Supplementary Table 5**.

Crystallisation and structure determination of Fab1

Fab1 at 6.5 mg/mL was crystallised by the sitting drop vapour diffusion method in 96-well SWISSCI 3-drop plates at 20°C. Drops consisted of 100 nL protein and 100 nL crystallisation solution were dispensed using a Mosquito robot (TTP Labtech). Crystals were grown in 0.16 M lithium chloride, 22% (*w/v*) PEG6000, 0.1 M MES pH 6.0 and were harvested after 21 days. Crystals were cryo-protected in the crystallisation solution supplemented with 20% (*v/v*) ethylene glycol before flash-cooling into liquid nitrogen. X-ray data were collected at Diamond Light Source on beamline I24 from a single cryo-cooled crystal (100 K) using a Pilatus3 6M detector. Diffraction data were collected for a total of 180° up to a resolution of 2.5 Å with a 0.2° oscillation using an exposure time of 0.04 seconds at 100% transmission. X-ray diffraction data were indexed and integrated by autoPROC and STARANISO[76] and were scaled to 2.96 Å in Aimless[77] using the I24 beamline autoprocessing pipeline. The crystals belonged to a monoclinic space group $P12_11$ with unit cell parameters a = 92.0 Å, b = 130.1 Å, c = 138.9 Å, α = 90.00°, β = 106.1°, γ = 90.00°. The structure was solved by molecular replacement using Phaser[78] and the C_H domain of the anti-NFG Fab as the search model (PDB accession number 1ZAN[79]). Crystallographic refinement was performed using PHENIX-1.9[72,80] and model building was carried out in *Coot*[73]. MolProbity[74] was used for structure validation and quality assessment. The final model coordinates and structure factors are deposited in the PDB under the accession number 7BM5.

Reconstitution of BamA and different BAM complexes into DMPC proteoliposomes

DMPC (*di*$C_{14:0}$PC), purchased as powder from Avanti Polar Lipids (Alabaster, AL), was dissolved in 80:20 (*v/v*) chloroform/methanol mixture at 25 mg/mL. Appropriate volumes were dried to thin films in clean Pyrex tubes at 42 °C under N_2 gas, and were further dried by vacuum desiccation for > 3 hours. BAM WT, BAM-LL and BAM-P5L or a 2:1 (*mol/mol*) mixture of Fab1 and BAM in TBS pH 8.0, 0.05% (*w/v*) DDM were mixed with DMPC lipid solubilized in TBS pH 8.0, 0.05% (*w/v*) DDM at a lipid to protein ratio (LPR) of 1600:1 (*mol/mol*). For BamA, DMPC lipid was first solubilised in TBS pH 8.0, 0.1% (*w/v*) LDAO. Empty liposomes were prepared by mixing DDM-solubilised lipid with an equivalent volume of buffer. Dialysis was performed as described for the preparation of *E. coli* polar lipid proteoliposomes, except that a temperature of 30 °C was used (above the DMPC transition temperature). Following dialysis, the proteoliposomes were pelleted twice by ultracentrifugation at 100,000 *g* for 30 min at 4 °C and resuspended in TBS pH 8.0. The proteoliposomes were then extruded with 21 passes through a 0.1 µm polycarbonate membrane using a mini-extruder (Avanti) pre-equilibrated at 30 °C. Following ultracentrifugation as before, proteoliposomes were resuspended in TBS pH 8.0, protein concentration was determined using a BCA assay (ThermoScientific) and successful reconstitution was confirmed using SDS-PAGE.

Probing lipid disorder using laurdan

Laurdan (Cambridge Bioscience) dissolved in DMSO was added to a final concentration of 4.2 µM (final DMSO concentration of 0.15% (*v/v*)) to a 0.8 µM suspension of BAM-, BamA- or empty-DMPC proteoliposomes (LPR 1600:1 mol/mol). The proteoliposomes were incubated at 25 °C overnight to allow random partitioning of the laurdan probe into the membrane. Fluorescence emission was measured at 440 nm and 490 nm for a total time of 10 sec following excitation of laurdan fluorescence at 340 nm in quartz cuvettes using a PTI QuantaMaster fluorimeter with a 1 nm bandwidth and 1 second integration time. Excitation and emission slit widths were set to 0.1 nm. Spectra were acquired at increasing temperature intervals from 6 °C to 40 °C, and to test reversibility, from 40 °C to 6 °C, allowing the sample to equilibrate at each temperature for 3 min. Generalised polarisation (GP)[46] was calculated from the ratio of fluorescence intensity at 440 nm and 490 nm, averaged over the 10 second acquisition, using the formula $GP = (I_{440}-I_{490})/(I_{440}+I_{490})$, and was plotted against temperature. Mid-points and gradients of the transitions were determined by calculating the first derivative of the curve.

Data availability

Raw micrographs for each dataset are deposited at EMPIAR under accession numbers XXXX (BAM-LL), XXXX (BAM Fab1 complex), XXXX (BAM-P5L), XXXX (BAM-LL Fab1 complex). The final density maps are deposited in the EMDB under accession numbers XXXX (BAM-LL lateral-closed), XXXX (BAM-LL lateral-open), XXXX (BAM Fab1 complex), XXXX (BAM-P5L) and XXXX (BAM-LL Fab1 complex). Final model coordinates have been deposited in the PDB under accession numbers XXXX (BAM-LL lateral-closed), XXXX (BAM-LL lateral-open), XXXX (BAM Fab1 complex) and XXXX (BAM-LL Fab1 complex). The crystal structure of Fab1 has been deposited in the PDB under accession number 7BM5, and crystallographic data are available at https://doi.org/10.2210/pdb7BM5/pdb. Data supporting this study are freely available at the University of Leeds Data Repository: https://doi.org/10.5518/835.

Acknowledgements

We thank members of the Radford, Ranson, Brockwell and Rutherford labs for helpful discussions, and Nasir Khan for technical support. CryoEM data were collected at the Astbury Biostructure Laboratory, funded by the University of Leeds and the Wellcome Trust (108466/Z/15/Z). We thank Diamond Light Source for access to Beamline i24 (MX19248). P.W and M.G.I acknowledge funding from the Medical Research Council UK

(MR/P018491/1). S.H and J.E.H are funded by the White Rose BBSRC DTP (BB/M011151/1) J.M. and A.J.H acknowledge support from the Wellcome Trust (222373/Z/21/Z and 105220/Z/14/Z, respectively). B.S acknowledges support from the BBSRC (BB/N007603/1 and BB/T000635/1). For the purpose of Open Access, the authors have applied a CC BY public copyright licence to any Author Accepted Manuscript version arising from this submission. J.W. is funded by an EOS Excellence in Research Program of the FWO and FRS-FNRS (G0G0818N). SER holds a Royal Society Professorial Fellowship (RSRP/R1/211057).

Author contributions

P.W, S.F.H, M.G.I and A.J.H designed and performed the experiments and analysed the data. P.W, S.F.H, J.M.M, A.J.H, B.S and C.C.P carried out BAM functional assays. P.W prepared protein samples for cryoEM. S.F.H, M.G.I and J.M.M performed cryoEM experiments and determined BAM cryoEM structures. P.W solved the X-ray structure of Fab1. P.W, S.F.H, J.E.H, B.S, C.C.P and J.M.W produced proteins required for the study. J.E.H developed the BAM laurdan fluorescence assay. K.M.S and S.T.R developed and produced the anti-BamA Fab fragment (Fab1). S.E.R, N.A.R and D.J.B supervised the research. P.W, S.F.H and M.G.I wrote the manuscript with comments and edits provided from all authors.

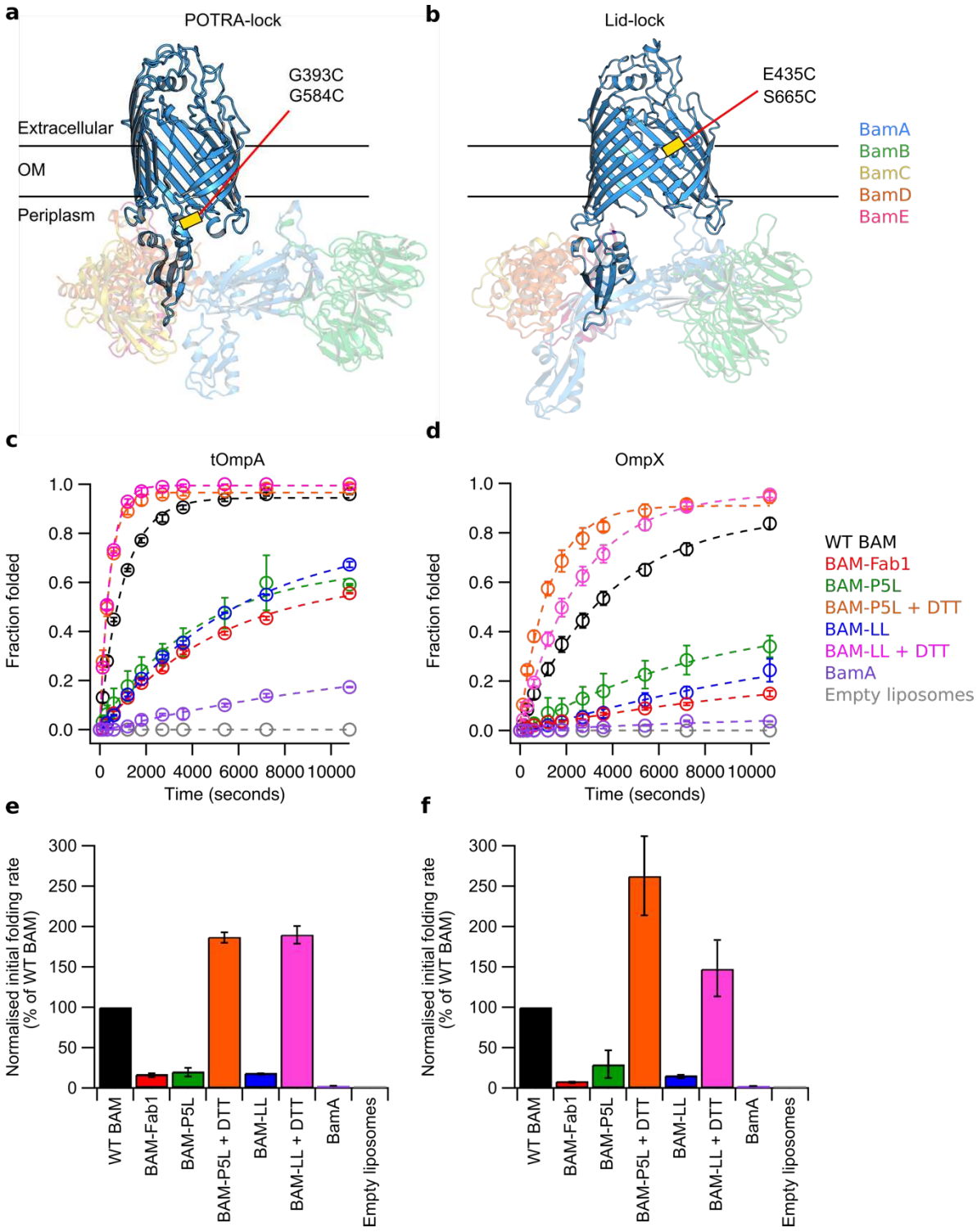

Fig. 1 | Disulphide-locked BamA variants and Fab1 binding impair BAM-mediated OMP folding *in vitro*. (a) BAM-P5L (G393C/G584C) is expected to lock BamA in the lateral-open conformation (PDB code 5LJO[8]), while **(b)** BAM-LL (E435C/S665C) is expected to lock BamA in the lateral-closed conformation (PDB code 5D0O[6]). BamA POTRAs 1-4 and BamBCDE are rendered semi-transparent for emphasis on the BamA β-barrel and POTRA-5. The position of the disulphide bond is shown as a yellow bar. Figure made in PyMOL v1.7.2.3. (**c and d**) Quantification of folded and unfolded bands from SDS-PAGE band-shift

assays (**Supplementary Figs. 3 and 4**) plotted as fraction folded against time for tOmpA or OmpX, respectively. Data are fitted to a single exponential function. **(e and f)** The initial rates of folding (determined by applying a linear fit to the first 5% of folding data) normalised as a percentage of the initial rate obtained for WT BAM, are shown for **(e)** tOmpA and **(f)** OmpX folding (see also **Supplementary Table 1**). Folding assays were repeated to assess reproducibility, with errors for replicate initial rate measurements listed in **Supplementary Table 1**. Folding yields after 24 hours are reported in **Supplementary Table 2**. Figures labelled with “BAM” refer to the full BAM complex (BamABCDE), whilst “BamA” is just BamA alone.

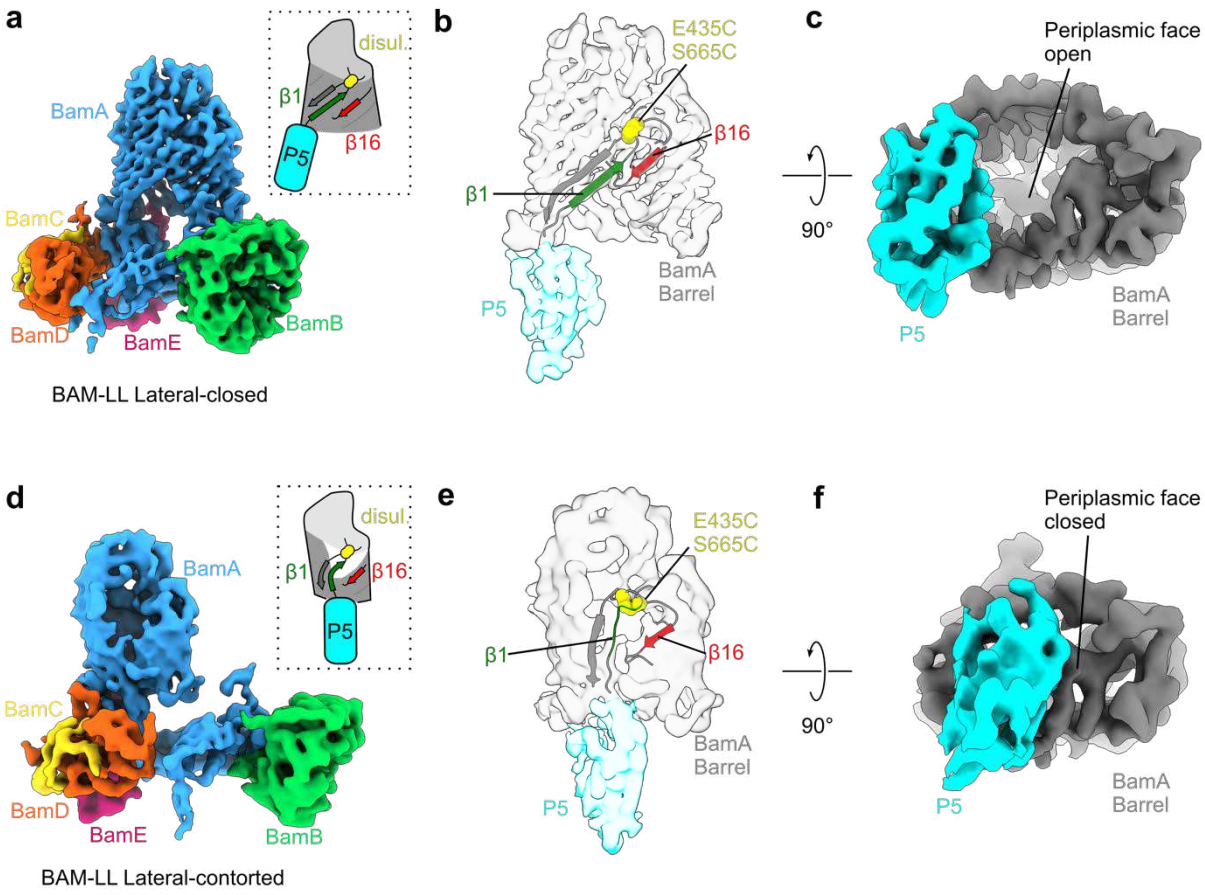

Fig. 2 | CryoEM resolves two conformations of BAM-LL in detergent. (**a**) 4.1 Å cryoEM map of the BAM-LL lateral-closed conformation at a contour of 10 σ, coloured by subunit. The lateral-gate is closed and POTRA-5 does not block the BamA barrel (schematic inset). (**b**) Cartoon representation of the corresponding atomic model at the lateral gate, superimposed on the segmented density for the barrel and POTRA-5 of BamA. β1 and β16 contact to close the gate. (**c**) The same density viewed from the periplasmic side, showing the open lumen of the BamA barrel in this conformation. (**d**) 4.8 Å cryoEM map of the BAM-LL lateral-open conformation at a contour of 10 σ, coloured by subunit. The lateral-gate is open and POTRA-5 occludes the BamA barrel (schematic inset). (**e**) Cartoon representation of the corresponding atomic model at the lateral gate, superimposed on segmented density for the barrel and POTRA-5 of BamA. To satisfy the disulphide in this conformation, eL1 must bend back into the barrel to contact eL6. (**f**) The same density viewed from the periplasmic side, showing that the BamA lumen is blocked by POTRA-5 in this conformation. Fig. made in UCSF ChimeraX[76]. Segmenting and colouring performed with corresponding atomic models. Less well resolved regions and the micelle have been masked.

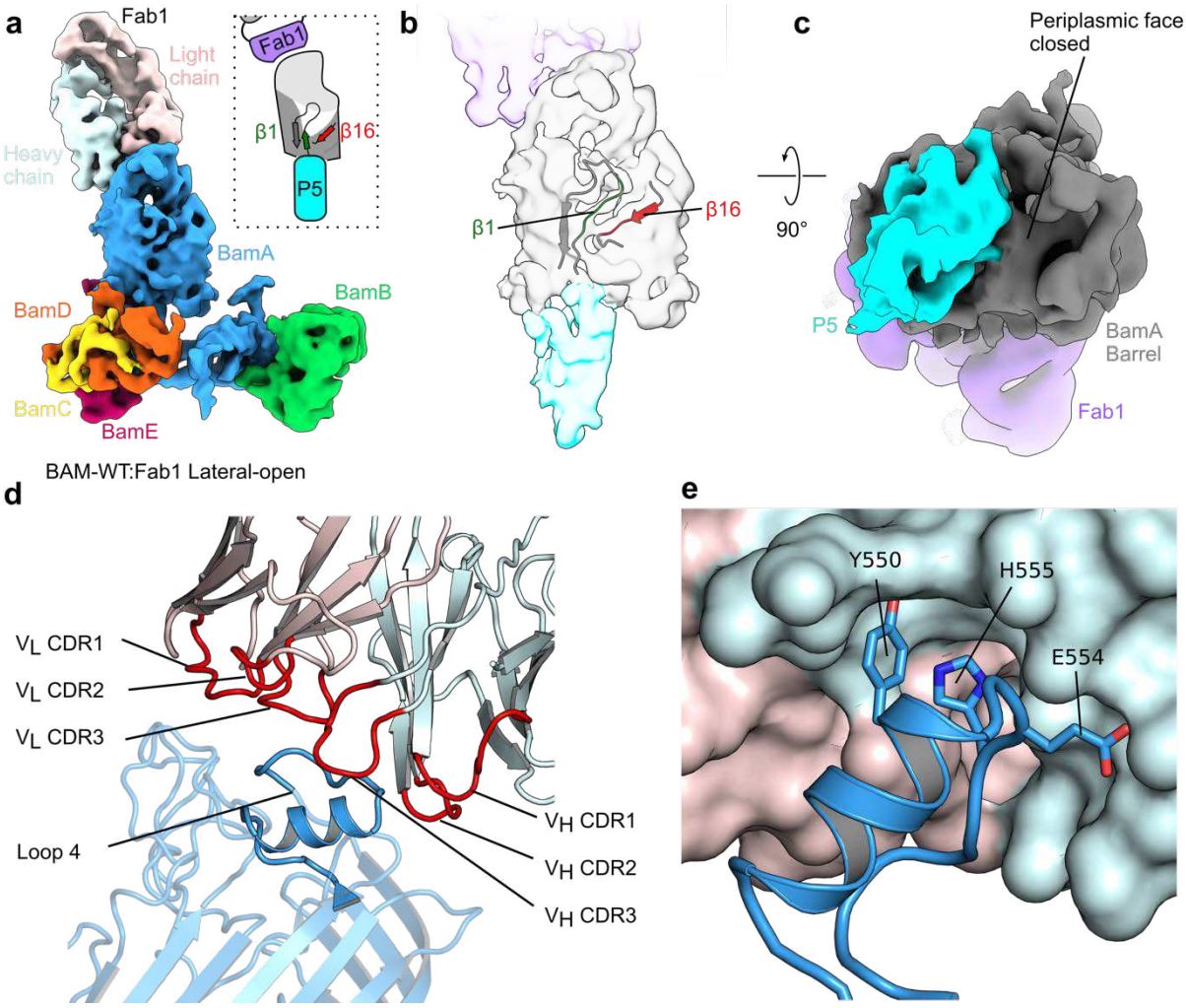

Fig. 3 | **Fab1-bound BAM is in a lateral-open conformation. (a)** 5.1 Å cryoEM map of the BAM-Fab1 complex in a lateral-open conformation at a contour of 10 σ, coloured by subunit. The lateral-gate is fully-open and POTRA-5 occludes the BamA barrel (*schematic inset*). **(b)** Cartoon representation of the corresponding atomic model at the lateral gate, superimposed on the segmented density for the barrel and POTRA-5 of BamA. β1 is in a conformation that makes limited contact with β16. **(c)** The same density viewed from the periplasmic side, showing that the BamA lumen is blocked by POTRA-5 in this conformation. Panels made using UCSF ChimeraX[76]. Segmenting and colouring performed with corresponding atomic models. Less well resolved regions and the micelle have been masked. **(d)** Close up of the BamA-Fab1 interface region highlighting the Fab1 CDRs (*red*) interacting with eL4 of BamA (*dark blue).* Other regions of BamA are rendered semi-transparent to highlight eL4. Heavy and light chains of Fab1 are coloured *cyan* and *pink*, respectively. (**e**) The V_L and V_H domains of Fab1 variable form a complementary binding surface for eL4 of BamA involving residues Y550, E554 and H555.

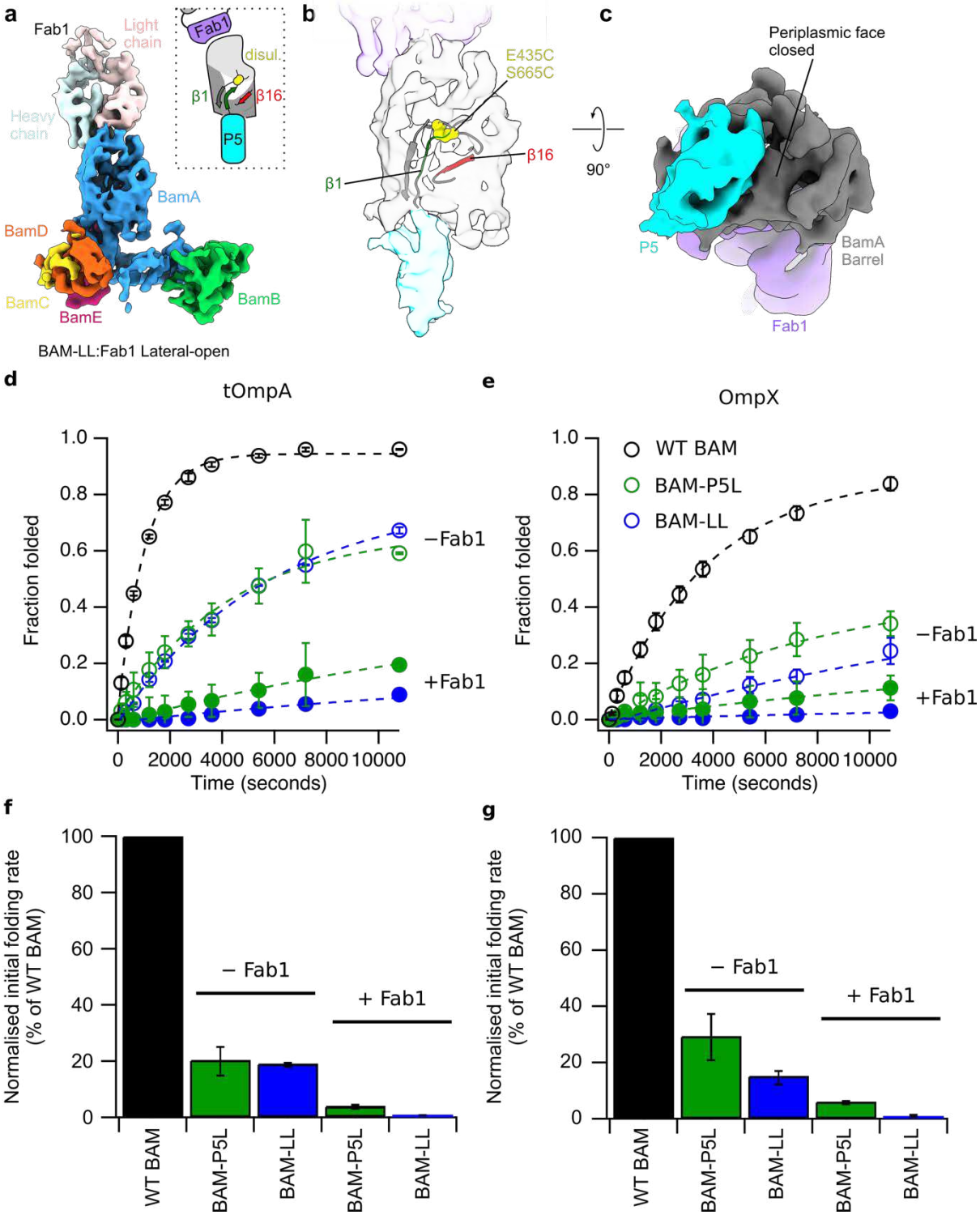

Fig. 4 | Additive effect of BAM inhibition by disulphide-locking and binding of Fab1. **(a)** 7.1 Å cryoEM map of the Fab1-bound LL-BAM in a lateral-open conformation at a contour of 9.5 σ, coloured by subunit. The lateral-gate is open and POTRA-5 occludes the BamA barrel (schematic inset). **(b)** Cartoon representation of the corresponding atomic model at the lateral gate, superimposed on the segmented density for the β-barrel and

POTRA-5 of BamA. To satisfy the disulphide in this conformation, eL1 must bend back into the barrel to contact eL6. **(c)** The same density viewed from the periplasmic side, showing that the BamA lumen is blocked by POTRA-5 in this conformation. Structural panels made using UCSF ChimeraX[76]. Segmenting and colouring performed with corresponding atomic models. Less well resolved regions and the micelle have been masked. **(d and e)** Quantification of SDS-PAGE band-shift assays shown in **Supplementary Fig. 13** for **(d)** tOmpA and **(e)** OmpX folding catalysed by BAM-P5L (*green*), BAM-LL (*blue*) and WT BAM (*black*), each with and without Fab1 (*solid and open circles, respectively*)**.** (**f and g**) The initial rates, calculated by applying a linear fit to the first 5% of fitted folding data, were normalised to that of WT BAM, and are shown for **(f)** tOmpA and **(g)** OmpX folding (see also **Supplementary Table 1**). Folding assays were conducted twice for reproducibility with data for replicate initial rate measurements listed in **Supplementary Table 1.** Folding yields after 24 hours are reported in **Supplementary Table 2**. Figures labelled with "BAM" refer to the full BAM complex (BamABCDE).

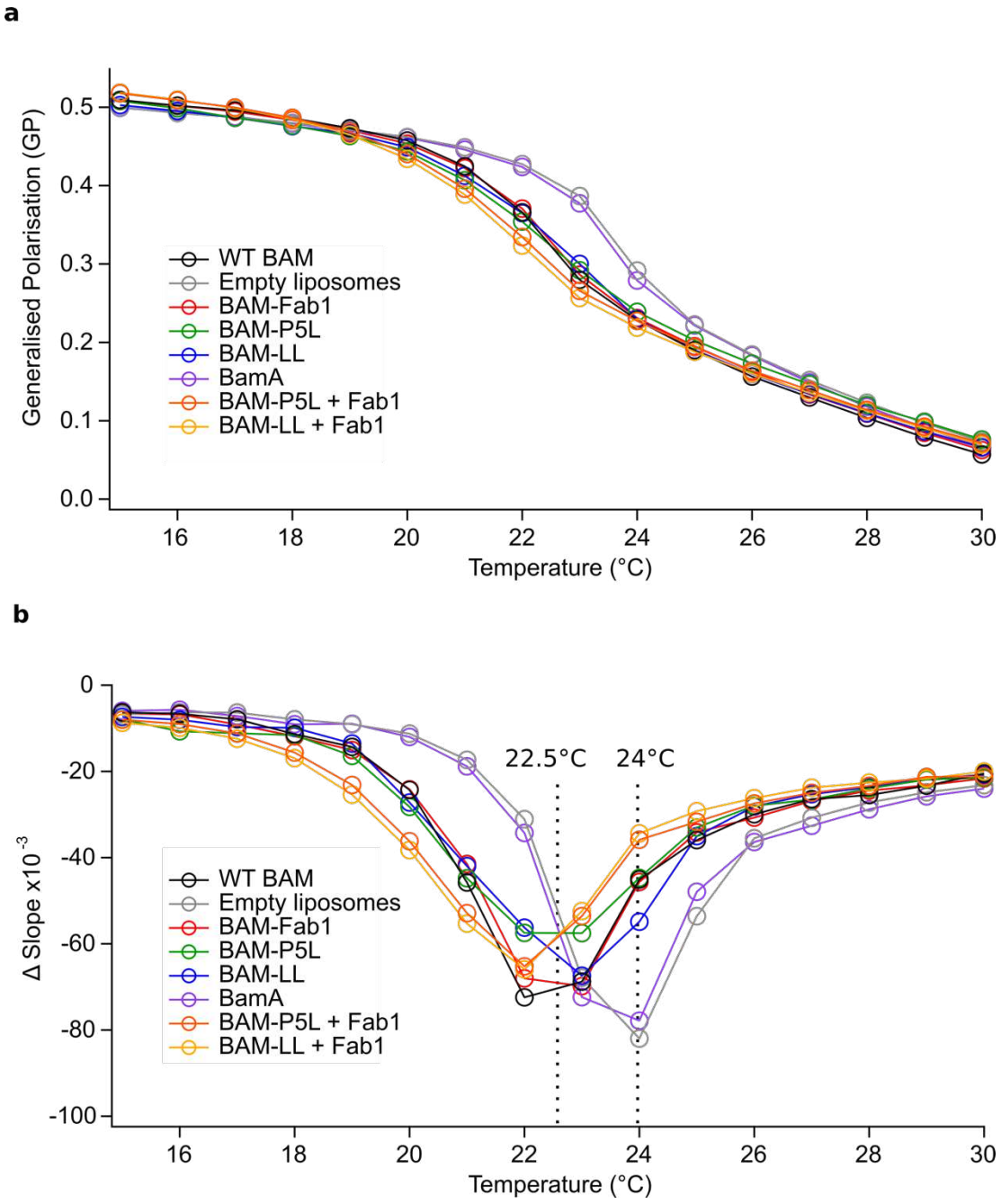

Fig. 5 | BAM variants reduce the phase transition temperature of DMPC liposomes. Global lipid phase transition behaviour for each BAM variant and BamA in DMPC proteoliposomes, with an empty liposomes control measured using laurdan fluorescence. **(a)** The ratio of laurdan fluorescence at 440 nm and 490 nm was plotted as generalised polarisation (GP, *see Methods*) against temperature for 0.8 µM BAM/BamA proteoliposome suspensions at a 1600:1 (mol/mol) lipid-to-protein ratio (LPR) with added laurdan (at a 305:1 lipid-to-laurdan ratio) in TBS pH 8.0. **(b)** The first derivative of data shown in **(a)** showing the transition temperature for each liposome suspension as the point of steepest (most negative) gradient. Whilst empty DMPC (*grey*) and BamA proteoliposomes (*purple*) have a transition temperature of 24 °C, the presence of WT BAM (*black*), BAM-Fab1 (*red*), BAM-P5L (*green*), BAM-LL (*blue*), BAM-P5L + Fab1 *(orange)* and BAM-LL + Fab1 *(yellow)*

broaden the phase transition and lower the transition temperature. Figures labelled with "BAM" refer to the full BAM complex (BamABCDE), whilst "BamA" is just BamA alone.

References

1. Horne, J. E., Brockwell, D. J. & Radford, S. E. Role of the lipid bilayer in outer membrane protein folding in Gram-negative bacteria. *J. Biol. Chem*. **295**, 10340–10367 (2020).
2. Noinaj, N., Gumbart, J. C. & Buchanan, S. K. The β-barrel assembly machinery in motion. *Nat. Rev. Microbiol*. **15**, 197–204 (2017).
3. Konovalova, A., Kahne, D. E. & Silhavy, T. J. Outer membrane biogenesis. *Annu. Rev. Microbiol*. **71**, 539–556 (2017).
4. Voulhoux, R., Bos, M. P., Geurtsen, J., Mols, M. & Tommassen, J. Role of a highly conserved bacterial protein in outer membrane protein assembly. *Science* **299**, 262–265 (2003).
5. Bakelar, J., Buchanan, S. K. & Noinaj, N. The structure of the β-barrel assembly machinery complex. *Science* **351**, 180–186 (2016).
6. Gu, Y. *et al*. Structural basis of outer membrane protein insertion by the BAM complex. *Nature* **531**, 64 (2016).
7. Han, L. *et al*. Structure of the BAM complex and its implications for biogenesis of outer-membrane proteins. *Nat. Struct. Mol. Biol*. **23**, 192–196 (2016).
8. Iadanza, M. G. *et al*. Lateral opening in the intact β-barrel assembly machinery captured by cryo-EM. *Nat. Commun*. **7**, 12865 (2016).
9. Hart, E. M., Gupta, M., Wühr, M. & Silhavy, T. J. The synthetic phenotype of ΔBamB ΔBamE double mutants results from a lethal jamming of the BAM complex by the lipoprotein RcsF. *MBio* **10**, (2019).
10. Tata, M. & Konovalova, A. Improper coordination of BamA and BamD results in BAM complex jamming by a lipoprotein substrate. *MBio* **10**, (2019).
11. Luther, A. *et al*. Chimeric peptidomimetic antibiotics against Gram-negative bacteria. *Nature* **576,** 452-458 (2019).
12. Imai, Y. *et al*. A new antibiotic selectively kills Gram-negative pathogens. *Nature* **576,** 459-464 (2019).
13. Hart, E. M. *et al*. A small-molecule inhibitor of BamA impervious to efflux and the outer membrane permeability barrier. *Proc. Natl. Acad. Sci. U.S.A.* **116**, 21748–21757 (2019).
14. Urfer, M. *et al*. A peptidomimetic antibiotic targets outer membrane proteins and disrupts selectively the outer membrane in *Escherichia coli*. *J. Biol. Chem*. **291**, 1921–32 (2016).
15. Hagan, C. L., Wzorek, J. S. & Kahne, D. Inhibition of the β-barrel assembly machine by a peptide that binds BamD. *Proc. Natl. Acad. Sci. U.S.A*. **112**, 2011–6 (2015).
16. Storek, K. M. *et al*. Monoclonal antibody targeting the β-barrel assembly machine of *Escherichia coli* is bactericidal. *Proc. Natl. Acad. Sci. U.S.A.* **115**, 3692–3697 (2018).
17. Kaur, H. *et al*. Identification of conformation-selective nanobodies against the membrane protein insertase BamA by an integrated structural biology approach. *J. Biomol. NMR* **73**, 375–384 (2019).
18. Iadanza, M. G. *et al*. Distortion of the bilayer and dynamics of the BAM complex in lipid nanodiscs. *Commun. Biol*. **3**, 766 (2020).
19. Noinaj, N., Kuszak, A. J., Balusek, C., Gumbart, J. C. & Buchanan, S. K. Lateral opening and exit pore formation are required for BamA function. *Structure* **22**, 1055–

1062 (2014).

20. Doerner, P. A. & Sousa, M. C. Extreme dynamics in the BamA β-barrel seam. *Biochemistry* **56**, 3142–3149 (2017).

21. Rodríguez-Alonso, R. *et al*. Structural insight into the formation of lipoprotein-β-barrel complexes. *Nat. Chem. Biol*. **16**, 1019–1025 (2020).

22. Xiao, L. *et al*. Structures of the β-barrel assembly machine recognizing outer membrane protein substrates. *FASEB J.* **35**, e21207 (2021).

23. Warner, L. R., Gatzeva-Topalova, P. Z., Doerner, P. A., Pardi, A. & Sousa, M. C. Flexibility in the periplasmic domain of BamA is important for function. *Structure* **25**, 94–106 (2017).

24. Lundquist, K., Billings, E., Bi, M., Wellnitz, J. & Noinaj, N. The assembly of β-barrel membrane proteins by BAM and SAM. *Mol. Microbiol*. (2020).

25. Schiffrin, B., Brockwell, D. J. & Radford, S. E. Outer membrane protein folding from an energy landscape perspective. *BMC Biol*. **15**, 123 (2017).

26. Höhr, A. I. C. *et al*. Membrane protein insertion through a mitochondrial β-barrel gate. *Science*. **359**, (2018).

27. Doyle, M. T. & Bernstein, H. D. Bacterial outer membrane proteins assemble via asymmetric interactions with the BamA β-barrel. *Nat. Commun*. **10**, 3358 (2019).

28. Lee, J. *et al*. Formation of a β-barrel membrane protein is catalyzed by the interior surface of the assembly machine protein BamA. *Elife* **8**, (2019).

29. Tomasek, D. *et al*. Structure of a nascent membrane protein as it folds on the BAM complex. *Nature* **583**, 473-478 (2020).

30. Noinaj, N. *et al*. Structural insight into the biogenesis of β-barrel membrane proteins. *Nature* **501**, 385–390 (2013).

31. Schiffrin, B. *et al*. Effects of periplasmic chaperones and membrane thickness on BamA-catalyzed outer-membrane protein folding. *J. Mol. Biol*. **429,** 3776-3792 (2017).

32. Liu, J. & Gumbart, J. C. Membrane thinning and lateral gating are consistent features of BamA across multiple species. *PLOS Comput. Biol*. **16**, e1008355 (2020).

33. Patel, G. J. & Kleinschmidt, J. H. The lipid bilayer-inserted membrane protein BamA of *Escherichia coli* facilitates insertion and folding of outer membrane protein A from its complex with Skp. *Biochemistry* **52,** 3794-3986 (2013).

34. Gessmann, D. *et al*. Outer membrane β-barrel protein folding is physically controlled by periplasmic lipid head groups and BamA. *Proc. Natl. Acad. Sci. U.S.A.* **111**, 5878–83 (2014).

35. Tiwari, P. B. & Mahalakshmi, R. Interplay of protein primary sequence, lipid membrane, and chaperone in β-barrel assembly. *Protein Sci*. (2021).

36. Rigel, N. W., Ricci, D. P. & Silhavy, T. J. Conformation-specific labelling of BamA and suppressor analysis suggest a cyclic mechanism for β-barrel assembly in *Escherichia coli. Proc. Natl. Acad. Sci. U.S.A.* **110**, 5151–5156 (2013).

37. Storek, K. M. *et al*. The *Escherichia coli* β-barrel assembly machinery is sensitized to perturbations under high membrane fluidity. *J. Bacteriol*. **201**, e00517-18 (2019).

38. Schüßler A., Herwig S., Kleinschmidt J.H. (2019) Kinetics of Insertion and Folding of Outer Membrane Proteins by Gel Electrophoresis. In: Kleinschmidt J. (eds) Lipid-Protein Interactions. Methods in Molecular Biology, vol 2003. Humana, New York, NY.

39. Hagan, C. L., Westwood, D. B. & Kahne, D. Bam lipoproteins assemble BamA *in vitro*.

885 *Biochemistry* **52**, 6108-6113 (2013).

886 40. Trabuco, L. G., Villa, E., Mitra, K., Frank, J. & Schulten, K. Flexible fitting of atomic
887 structures into electron microscopy maps using molecular dynamics. *Structure* **16**,
888 673–683 (2008).

889 41. Krissinel, E. Stock-based detection of protein oligomeric states in jsPISA. *Nucleic*
890 *Acids Res.* **43**, W314–W319 (2015).

891 42. Kleinschmidt, J. H. Folding of β-barrel membrane proteins in lipid bilayers —
892 Unassisted and assisted folding and insertion. *Biochim. Biophys. Acta - Biomembr.*
893 **1848**, 1927–1943 (2015).

894 43. Burgess, N. K., Dao, T. P., Stanley, A. M. & Fleming, K. G. β-barrel proteins that
895 reside in the *Escherichia coli* outer membrane *in vivo* demonstrate varied folding
896 behavior *in vitro*. *J. Biol. Chem.* **283**, 26748–26758 (2008).

897 44. Andersen, K. K., Wang, H. & Otzen, D. E. A kinetic analysis of the folding and
898 unfolding of OmpA in urea and guanidinium chloride: Single and parallel pathways.
899 *Biochemistry* **51**, 8371–8383 (2012).

900 45. Danoff, E. J. & Fleming, K. G. Membrane defects accelerate outer membrane β-barrel
901 protein folding. *Biochemistry* **54**, 97–99 (2015).

902 46. Parasassi, T., De Stasio, G., Ravagnan, G., Rusch, R. M. & Gratton, E. Quantitation
903 of lipid phases in phospholipid vesicles by the generalized polarization of Laurdan
904 fluorescence. *Biophys. J.* **60**, 179–89 (1991).

905 47. Bonora, S., Markarian, S. A., Trinchero, A. & Grigorian, K. R. DSC study on the effect
906 of dimethysulfoxide (DMSO) and diethylsulfoxide (DESO) on phospholipid liposomes.
907 *Thermochim. Acta* **433**, 19–26 (2005).

908 48. Hussain, S. & Bernstein, H. D. The Bam complex catalyzes efficient insertion of
909 bacterial outer membrane proteins into membrane vesicles of variable lipid
910 composition. *J. Biol. Chem.* **293**, 2959–2973 (2018).

911 49. Konovalova, A. *et al*. Inhibitor of intramembrane protease RseP blocks the σE
912 response causing lethal accumulation of unfolded outer membrane proteins. *Proc.*
913 *Natl. Acad. Sci. U.S.A.* **115**, E6614–E6621 (2018).

914 50. Dartigalongue, C., Missiakas, D. & Raina, S. Characterization of the *Escherichia coli*
915 σE regulon. *J. Biol. Chem.* **276**, 20866–20875 (2001).

916 51. Johansen, J., Rasmussen, A. A., Overgaard, M. & Valentin-Hansen, P. Conserved
917 small non-coding RNAs that belong to the σE regulon: Role in down-regulation of
918 outer membrane proteins. *J. Mol. Biol.* **364**, 1–8 (2006).

919 52. Rhodius, V. A., Suh, W. C., Nonaka, G., West, J. & Gross, C. A. Conserved and
920 variable functions of the σE stress response in related genomes. *PLoS Biol.* **4**, 0043–
921 0059 (2006).

922 53. Rollauer, S. E., Sooreshjani, M. A., Noinaj, N. & Buchanan, S. K. Outer membrane
923 protein biogenesis in Gram-negative bacteria. Philosophical Transactions of the Royal
924 Society B: Biological Sciences **370**, (2015).

925 54. Webb, C. T. *et al*. Dynamic association of BAM complex modules includes surface
926 exposure of the lipoprotein BamC. *J. Mol. Biol.* **422**, 545–555 (2012).

927 55. Lee, J. *et al*. Substrate binding to BamD triggers a conformational change in BamA to
928 control membrane insertion. *Proc. Natl. Acad. Sci. U.S.A.* **115**, 2359 LP – 2364
929 (2018).

930 56. Gunasinghe, S. D. *et al*. The WD40 protein BamB mediates coupling of BAM
931 complexes into assembly precincts in the bacterial outer membrane. *Cell Rep.* **23**,

2782–2794 (2018).

57. Ricci, D. P., Hagan, C. L., Kahne, D. & Silhavy, T. J. Activation of the *Escherichia coli* β-barrel assembly machine (Bam) is required for essential components to interact properly with substrate. *Proc. Natl. Acad. Sci. U.S.A.* **109**, 3487-3491 (2012).

58. Roman-Hernandez, G., Peterson, J. H. & Bernstein, H. D. Reconstitution of bacterial autotransporter assembly using purified components. *Elife* **3**, e04234 (2014).

59. Hartmann, J.-B., Zahn, M., Burmann, I. M., Bibow, S. & Hiller, S. Sequence-specific solution NMR assignments of the β-barrel insertase BamA to monitor its conformational ensemble at the atomic level. *J. Am. Chem. Soc.* **140,** 11252-11260 (2018).

60. Calabrese, A. N. *et al*. Inter-domain dynamics in the chaperone SurA and multi-site binding to its outer membrane protein clients. *Nat. Commun.* **11**, 1–16 (2020).

61. Simmons, L. C. *et al*. Expression of full-length immunoglobulins in *Escherichia coli*: Rapid and efficient production of aglycosylated antibodies. *J. Immunol. Methods*, **263,** 133-147 (2002).

62. Lombana, T. N., Dillon, M., Bevers, J. & Spiess, C. Optimizing antibody expression by using the naturally occurring framework diversity in a live bacterial antibody display system. *Sci. Rep.* (2015).

63. Zivanov, J. *et al*. New tools for automated high-resolution cryo-EM structure determination in RELION-3. *Elife* **7**, (2018).

64. Zivanov, J., Nakane, T. & Scheres, S. H. W. Estimation of high-order aberrations and anisotropic magnification from cryo-EM data sets in RELION-3.1. *IUCrJ* **7**, 253–267 (2020).

65. Zheng, S. Q. *et al*. MotionCor2: Anisotropic correction of beam-induced motion for improved cryo-electron microscopy. *Nat. Methods* **14**, 331–332 (2017).

66. Zhang, K. Gctf: Real-time CTF determination and correction. *J. Struct. Biol.* **193**, 1–12 (2016).

67. Wagner, T. *et al*. SPHIRE-crYOLO is a fast and accurate fully automated particle picker for cryo-EM. *Commun. Biol.* **2**, 1–13 (2019).

68. Punjani, A., Rubinstein, J. L., Fleet, D. J. & Brubaker, M. A. CryoSPARC: Algorithms for rapid unsupervised cryo-EM structure determination. *Nat. Methods* **14**, 290–296 (2017).

69. Punjani, A., Zhang, H. & Fleet, D. J. Non-uniform refinement: Adaptive regularization improves single particle cryo-EM reconstruction. *Nat. Methods* **17**, 1214-1221 (2020).

70. Henderson, R. *et al*. Outcome of the first electron microscopy validation task force meeting. in *Structure* **20**, 205–214 (2012).

71. Pettersen, E. F. *et al*. UCSF Chimera?A visualization system for exploratory research and analysis. *J. Comput. Chem*. **25**, 1605–1612 (2004).

72. Afonine, P. V. *et al*. Real-space refinement in PHENIX for cryo-EM and crystallography. *Acta Crystallogr. Sect. D Struct. Biol.* **74,** 531-544 (2018).

73. Emsley, P. & Cowtan, K. Coot: Model-building tools for molecular graphics. *Acta Crystallogr. Sect. D Biol. Crystallogr.* **60,** 2126-2132 (2004).

74. Chen, V. B. *et al*. MolProbity: All-atom structure validation for macromolecular crystallography. *Acta Crystallogr. Sect. D Biol. Crystallogr.* **66**, 12–21 (2010).

75. Kim, K. H., Aulakh, S. & Paetzel, M. Crystal structure of β-barrel assembly machinery BamCD protein complex. *J. Biol. Chem.* **286**, 39116–39121 (2011).

978 76. Tickle, I.J., Flensburg, C., Keller, P., Paciorek, W., Sharff, A. & Vonrhein, C.,
979 Bricogne, G. STARANISO. (2018).

980 77. Evans, P. R. & Murshudov, G. N. How good are my data and what is the resolution?
981 *Acta Crystallogr. D. Biol. Crystallogr.* **69**, 1204–1214 (2013).

982 78. McCoy, A. J. *et al*. Phaser crystallographic software. *J. Appl. Crystallogr.* **40**, 658–674
983 (2007).

984 79. Covaceuszach, S. *et al*. Dissecting NGF interactions with TrkA and p75 receptors by
985 structural and functional studies of an anti-NGF neutralizing antibody. *J. Mol. Biol.*
986 **381**, 881–896 (2008).

987 80. Adams, P. D. *et al*. PHENIX: A comprehensive Python-based system for
988 macromolecular structure solution. *Acta Crystallogr. Sect. D Biol. Crystallogr.* **66**,
989 213–221 (2010).

990

Figures

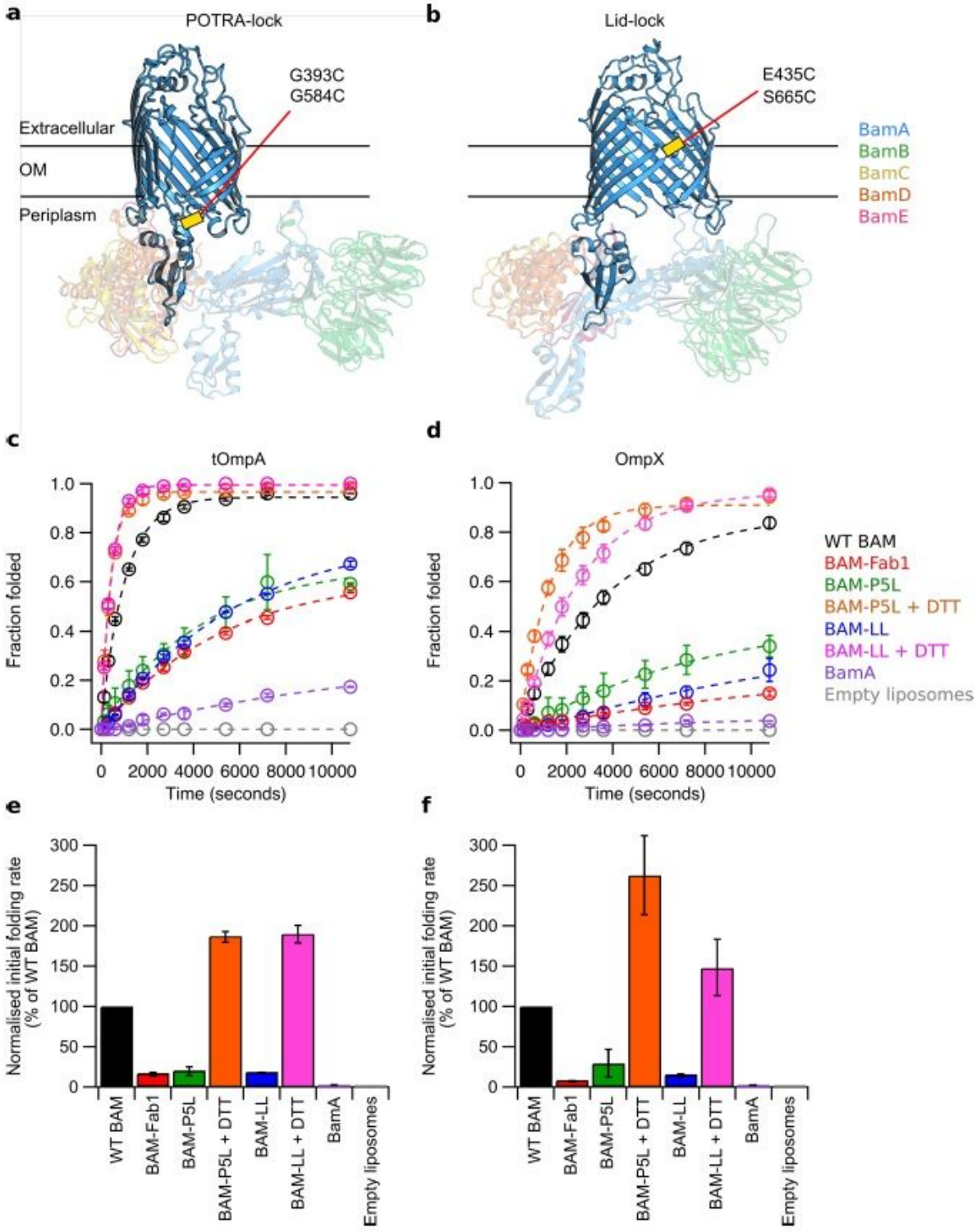

Figure 1

Disulphide-locked BamA variants and Fab1 binding impair BAM-mediated OMP folding in vitro. (a) BAM-P5L (G393C/G584C) is expected to lock BamA in the lateral- open conformation (PDB code 5LJO8), while (b) BAM-LL (E435C/S665C) is expected to lock BamA in the lateral-closed conformation (PDB code

5D0O6). BamA POTRAs 1-4 and BamBCDE are rendered semi-transparent for emphasis on the BamA β-barrel and POTRA-5. The position of the disulphide bond is shown as a yellow bar. Figure made in PyMOL v1.7.2.3. (c and d) Quantification of folded and unfolded bands from SDS-PAGE band-shift assays (Supplementary Figs. 3 and 4) plotted as fraction folded against time for tOmpA or OmpX, respectively. Data are fitted to a single exponential function. (e and f) The initial rates of folding (determined by applying a linear fit to the first 5% of folding data) normalised as a percentage of the initial rate obtained for WT BAM, are shown for (e) tOmpA and (f) OmpX folding (see also Supplementary Table 1). Folding assays were repeated to assess reproducibility, with errors for replicate initial rate measurements listed in Supplementary Table 1. Folding yields after 24 hours are reported in Supplementary Table 2. Figures labelled with “BAM” refer to the full BAM complex (BamABCDE), whilst “BamA” is just BamA alone.

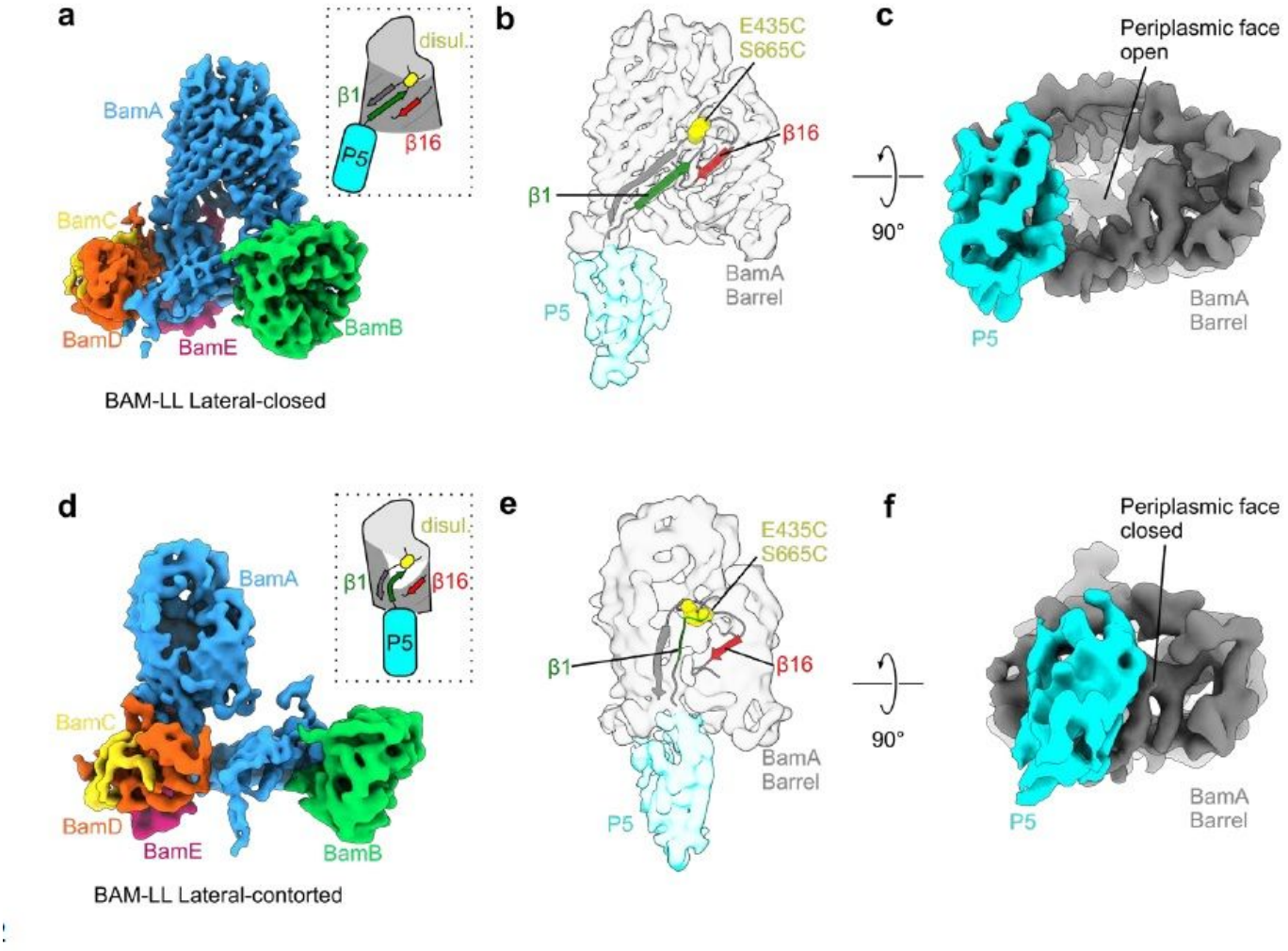

Figure 2

CryoEM resolves two conformations of BAM-LL in detergent. (a) 4.1 723 Å cryoEM map of the BAM-LL lateral-closed conformation at a contour of 10 σ, coloured by subunit. The lateral-gate is closed and POTRA-5 does not block the BamA barrel (schematic inset). (b) Cartoon representation of the corresponding atomic model at the lateral gate, superimposed on the segmented density for the barrel and POTRA-5 of BamA. β1 and β16 contact to close the gate. (c) The same density viewed from the

periplasmic side, showing the open lumen of the BamA barrel in this conformation. (d) 4.8 Å cryoEM map of the BAM- LL lateral-open conformation at a contour of 10 σ, coloured by subunit. The lateral-gate is open and POTRA-5 occludes the BamA barrel (schematic inset). (e) Cartoon representation of the corresponding atomic model at the lateral gate, superimposed on segmented density for the barrel and POTRA-5 of BamA. To satisfy the disulphide in this conformation, eL1 must bend back into the barrel to contact eL6. (f) The same density viewed from the periplasmic side, showing that the BamA lumen is blocked by POTRA-5 in this conformation. Fig. made in UCSF ChimeraX76. Segmenting and colouring performed with corresponding atomic models. Less well resolved regions and the micelle have been masked.

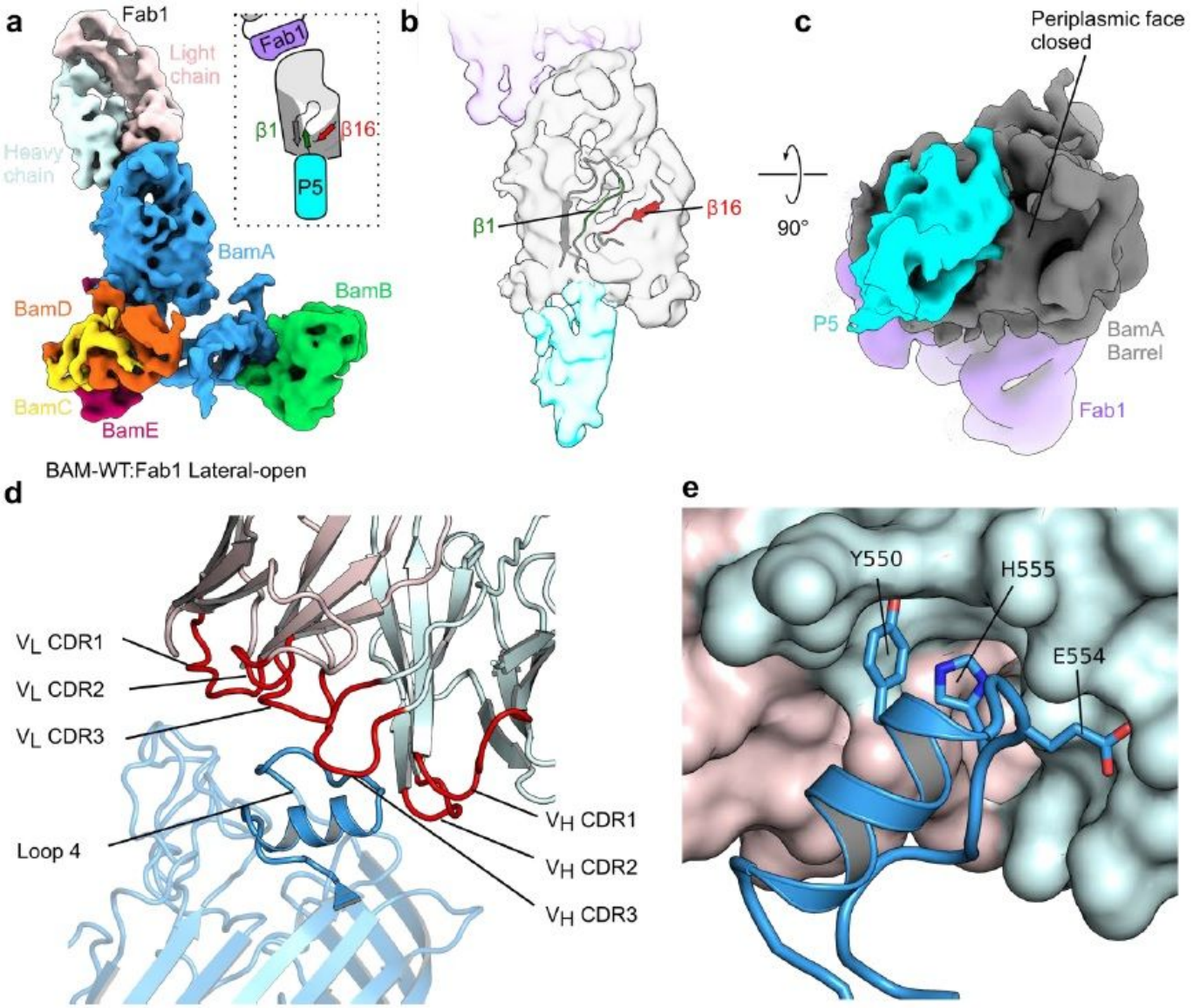

Figure 3

Fab1-bound BAM is in a lateral-open conformation. (a) 5.1 Å cryoEM map of the BAM-Fab1 complex in a lateral-open conformation at a contour of 10 σ, coloured by subunit. The lateral-gate is fully-open and

POTRA-5 occludes the BamA barrel (schematic inset). (b) Cartoon representation of the corresponding atomic model at the lateral gate, superimposed on the segmented density for the barrel and POTRA-5 of BamA. β1 is in a conformation that makes limited contact with β16. (c) The same density viewed from the periplasmic side, showing that the BamA lumen is blocked by POTRA-5 in this conformation. Panels made using UCSF ChimeraX76. Segmenting and colouring performed with corresponding atomic models. Less well resolved regions and the micelle have been masked. (d) Close up of the BamA-Fab1 interface region highlighting the Fab1 CDRs (red) interacting with eL4 of BamA (dark blue). Other regions of BamA are rendered semi-transparent to highlight eL4. Heavy and light chains of Fab1 are coloured cyan and pink, respectively. (e) The VL and VH domains of Fab1 variable form a complementary binding surface for eL4 of BamA involving residues Y550, E554 and H555.

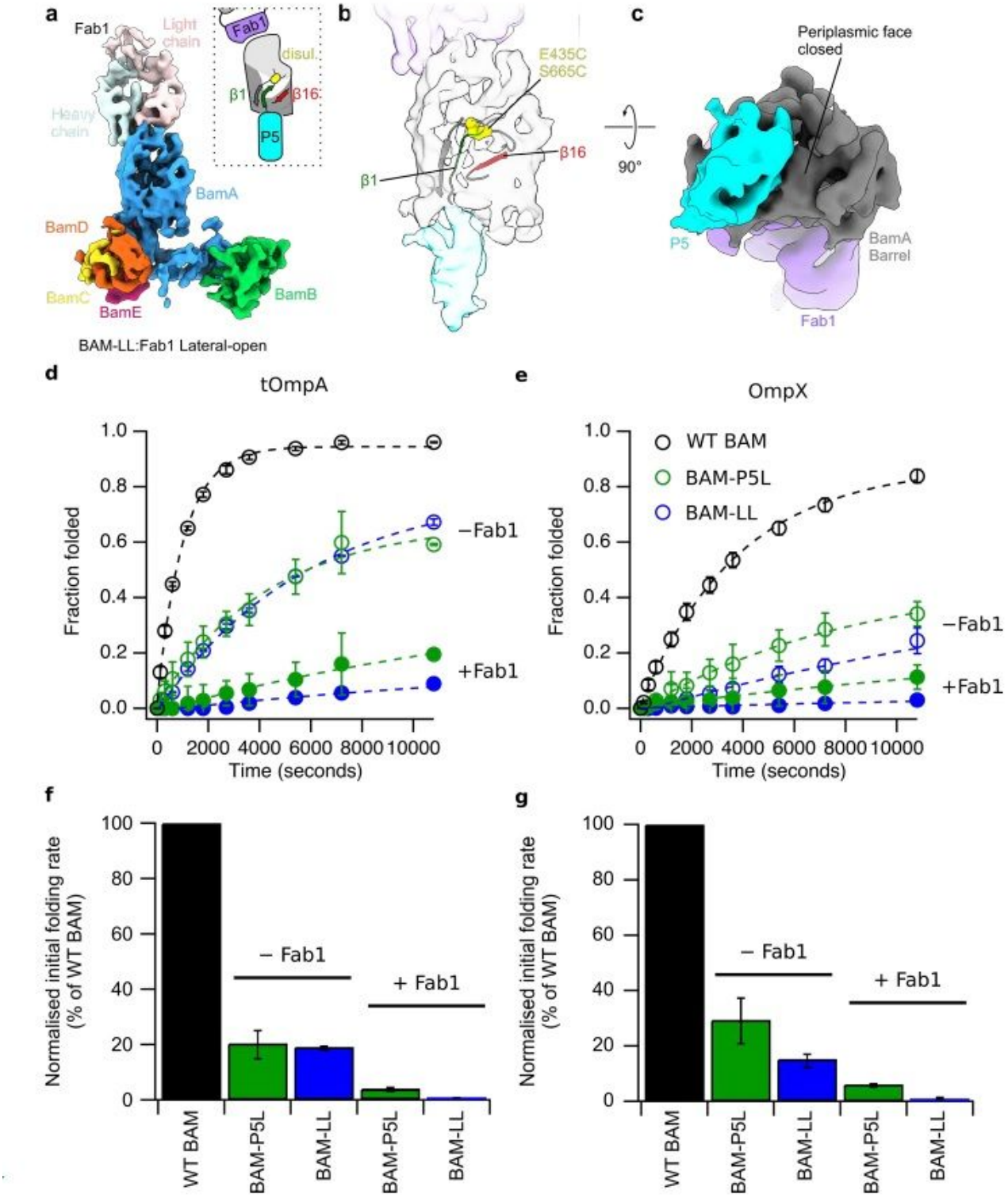

Figure 4

Additive effect of BAM inhibition by disulphide-locking and binding of Fab1. (a) 7.1 Å cryoEM map of the Fab1-bound LL-BAM in a lateral-open conformation at a contour of 9.5 σ, coloured by subunit. The lateral-gate is open and POTRA-5 occludes the BamA barrel (schematic inset). (b) Cartoon representation of the corresponding atomic model at the lateral gate, superimposed on the segmented density for the β-barrel and POTRA-5 of BamA. To satisfy the disulphide in this conformation, eL1 must bend back into the barrel

to contact eL6. (c) The same density viewed from the periplasmic side, showing that the BamA lumen is blocked by POTRA-5 in this conformation. Structural panels made using UCSF ChimeraX76. Segmenting and colouring performed with corresponding atomic models. Less well resolved regions and the micelle have been masked. (d and e) Quantification of SDS-PAGE band-shift assays shown in Supplementary Fig. 13 for (d) tOmpA and (e) OmpX folding catalysed by BAM-P5L (green), BAM-LL (blue) and WT BAM (black), each with and without Fab1 (solid and open circles, respectively). (f and g) The initial rates, calculated by applying a linear fit to the first 5% of fitted folding data, were normalised to that of WT BAM, and are shown for (f) tOmpA and (g) OmpX folding (see also Supplementary Table 1). Folding assays were conducted twice for reproducibility with data for replicate initial rate measurements listed in Supplementary Table 1. Folding yields after 24 hours are reported in Supplementary Table 2. Figures labelled with “BAM” refer to the full BAM complex (BamABCDE).

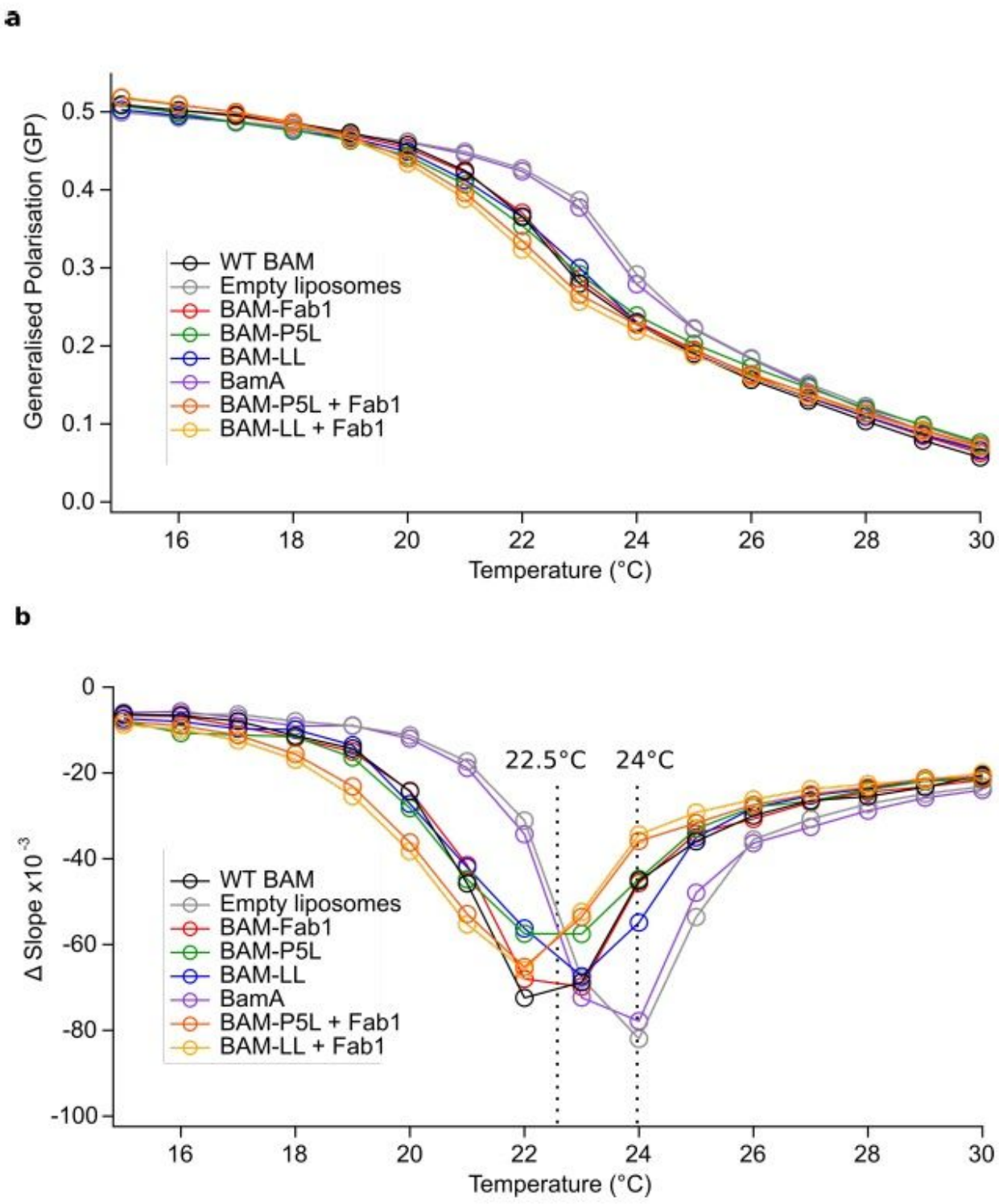

Figure 5

BAM variants reduce the phase transition temperature of DMPC liposomes. Global lipid phase transition behaviour for each BAM variant and BamA in DMPC proteoliposomes, with an empty liposomes control measured using laurdan fluorescence. (a) The ratio of laurdan fluorescence at 440 nm and 490 nm was plotted as generalised polarisation (GP, see Methods) against temperature for 0.8 μM BAM/BamA proteoliposome suspensions at a 1600:1 (mol/mol) lipid-to-protein ratio (LPR) with added laurdan (at a

305:1 lipid-to-laurdan ratio) in TBS pH 8.0. (b) The first derivative of data shown in (a) showing the transition temperature for each liposome suspension as the point of steepest (most negative) gradient. Whilst empty DMPC (grey) and BamA proteoliposomes (purple) have a transition temperature of 24 °C, the presence of WT BAM (black), BAM-Fab1 (red), BAM-P5L (green), BAM-LL (blue), BAM-P5L + Fab1 (orange) and BAM-LL + Fab1 (yellow) broaden the phase transition and lower the transition temperature. Figures labelled with “BAM” refer to the full BAM complex (BamABCDE), whilst “BamA” is just BamA alone.

Supplementary Files

This is a list of supplementary files associated with this preprint. Click to download.

- SupplementaryInformationsubmitted.pdf
- ValidationReports.pdf